Check for updates

Hydrological Processes

WILEY

RESEARCH ARTICLE OPEN ACCESS

The Impact of Model Resolution on the Water Balance of a Dryland Basin

E. A. Quichimbo[1,2] | M. B. Singer[1,2,3] | K. Michaelides[4] | R. Rosolem[5] | M. O. Cuthbert[1,3]

[1]School of Earth and Environmental Sciences, Cardiff University, Cardiff, UK | [2]Earth Research Institute, University of California Santa Barbara, Santa Barbara, California, USA | [3]Water Research Institute, Cardiff University, Cardiff, UK | [4]School of Geographical Sciences, University of Bristol, Bristol, UK | [5]University of Bristol, Faculty of Engineering, University Walk, Clifton, UK

Correspondence: E. A. Quichimbo (quichimbomiguitamaea@cardiff.ac.uk)

Received: 25 May 2026 | **Revised:** 12 September 2026 | **Accepted:** 28 September 2026

Keywords: calibration | drylands | ephemeral streams | focused recharge | transmission losses | water balance

ABSTRACT

The spatial and temporal resolution of hydrological models determine model performance and affect water partitioning into fluxes and water storage changes. This is especially important in dryland regions which exhibit dynamic hydrological processes (both spatially and temporally) driven by highly variable and heterogeneous rainfall events, and potential evapotranspiration which exceeds annual precipitation rates. However, it is still unclear how varying model resolutions may affect performance and introduce uncertainty in water balance partitioning. Here, we use a parsimonious dryland-specific process-based hydrological model, DRYP, to assess the impact of temporal and spatial resolution on the water balance fluxes and stores in a dryland basin. To achieve this, we performed numerical experiments using three model grid sizes (300 m, 1 km, 5 km) and three time-steps (15 min, 1 h, 1 day) with four different built-in infiltration equations (Philips, Green Ampt, Shaake, Upscaled Green Ampt). The analysis was performed in the Walnut Gulch Experimental Watershed, Arizona, USA, where long-term, high-resolution datasets are available for both model calibration and evaluation. Results showed that sub-daily time steps combined with spatial resolution of less than 1-km grid size yield the best representations (Nash Sutcliffe index, NSE > 0.55) of hydrological fluxes and stores such as streamflow, soil moisture, and actual evapotranspiration. Model parameterization also indicates that coarser spatial and temporal resolutions require lower effective saturated hydraulic conductivity, reflecting the smoothing of rainfall variability associated with spatial and temporal aggregation. The analysis also highlights the importance of near-channel processes, such as transmission losses in ephemeral streambeds and the role of the riparian zone in providing water for plants and for groundwater recharge. These results have important implications for the quantification of water partitioning in dryland environments in response to rainstorms, and provide guidance for how to parameterize large-scale models, which requires careful consideration to represent key hydrological processes of interest to the modeller.

1 | Introduction

Predicting water balance components under current and future climates is an important aspect of water resource management which requires reliable and robust hydrological models. Choices of temporal and spatial resolution in models are typically determined by the required model efficiency and the resolution of globally available gridded datasets. However, the resolution of model parameterisation affects the scale of water partitioning into fluxes and storage which control the water balance (Blöschl et al. 1995; Blöschl and Sivapalan 1995; Kipkemoi et al. 2021; Scheidegger et al. 2021) and therefore influences which hydrological processes become dominant over different temporal and spatial integrations (Barthel and Banzhaf 2016; K. Beven 2001,

This is an open access article under the terms of the Creative Commons Attribution License, which permits use, distribution and reproduction in any medium, provided the original work is properly cited.

© 2026 The Author(s). *Hydrological Processes* published by John Wiley & Sons Ltd.

1995, 1991; Blöschl and Sivapalan 1995; Fenicia et al. 2008; Merz et al. 2009). This is especially relevant in dryland regions, where the high temporal and spatial variability of rainfall and potential evapotranspiration interact with heterogeneous landscape characteristics to have a great impact on water partitioning and runoff (Dunkerley 2018; Michaelides and Wilson 2007; Osborn and Lane 1969; Pilgrim et al. 1988; Yair and Lavee 1982), streamflow regimes (Costigan et al. 2017; Cudennec et al. 2007; Singer and Michaelides 2017; Wilcox et al. 2008), groundwater recharge (Cuthbert et al. 2016; Qiu et al. 2025; Scanlon et al. 2006; Taylor et al. 2013), evapotranspiration (García et al. 2013; Kibler et al. 2023; Mayes et al. 2020), vegetation dynamics (Sabathier et al. 2021; Warter et al. 2020), sediment transport (Hooke 2019; Jaeger et al. 2017; Laronne and Reid 1993; Michaelides and Singer 2014; Singer and Michaelides 2014), and even landscape evolution (e.g., Chen et al. 2019).

Drylands are regions where climatic conditions are characterized by high rates of evapotranspiration and low annual precipitation, so the land surface is typically dry when rainfall occurs. In drylands, precipitation events are characterized by their high intensity, short duration, and high spatial variability (Goodrich et al. 1997; Pilgrim et al. 1988; Zoccatelli et al. 2019). Runoff occurs mainly as a result of infiltration excess (Hortonian) overland flow due to high precipitation intensity relative to infiltration rates, leading to the development of short-lived streamflow in localized ephemeral streams and discontinuous flow across catchment tributaries. The water table is typically deep below the streambed so these ephemeral streams leak water to the subsurface via transmission losses through porous stream beds, which reduces discharge downstream and contributes to groundwater recharge—a mechanism called focused recharge (Abdulrazzak 1995; Coes and Pool 2007; Goodrich et al. 2018; Quichimbo et al. 2023, 2020; Schreiner-McGraw et al. 2019; Shanafield and Cook 2014; Taylor et al. 2013). In contrast, diffuse recharge from infiltration of water through upland soils at the location of rainfall delivery may be limited due to the generally high soil water deficits and high rates of evapotranspiration (Stephens 1994; Wheater et al. 2007). The highly variable climatic conditions of dryland environments in both time and space result in a highly dynamic hydrological system. This poses great challenges for catchment models that seek to characterize key components of the dryland water balance (Green et al. 2011; Huang et al. 2017; Quichimbo et al. 2021). And this challenge grows when models scale up from basins to regions (e.g., land surface models) where model resolutions tend to coarsen for operational reasons. Therefore, it is important to understand how the spatial and temporal resolution of models and the representation of the main hydrological processes affect water balance fluxes and storage within dryland environments.

The selection of model temporal and spatial resolution has a great impact on the representation of the hydrological processes, model parameterization and ultimately the performance of any model (K. Beven 1995, 1991; Beven and Binley 1992; Blöschl 2001; Blöschl et al. 2007; Blöschl and Sivapalan 1995; Dimitrova-Petrova et al. 2020; Merz and Plate 1997; Merz et al. 2009; Wen et al. 2021). The spatial and temporal scale of the model may impact key hydrological processes such as precipitation (Blake et al. 2025; Goodrich et al. 1995; Kipkemoi et al. 2021), infiltration and runoff (Blake et al. 2025; Faurès et al. 1995; Goodrich et al. 1997), soil moisture and groundwater recharge (Baroni et al. 2017; Barthel and Banzhaf 2016; Kebede et al. 2021). However, there is currently limited guidance on which spatial and temporal model resolution to use to capture the key processes that influence the water balance for a particular place. This is needed not only to enhance the understanding and quantification of water partitioning in dryland regions, but also to investigate the implications of climate variability and anthropogenic changes on water fluxes and storage above and below ground (Cuthbert et al. 2019; Huang et al. 2017, 2015; IPCC6 2021; Ó Dochartaigh et al. 2010; Reynolds et al. 2007; Wang et al. 2017).

The development of ephemeral streamflow in drylands is highly dependent on runoff generation by infiltration-excess, which in turn is strongly dependent on rainfall characteristics, soil hydraulic properties, and antecedent soil moisture (Blake et al. 2025; Green and Ampt 1911; Stewart et al. 2019). When rainfall intensity exceeds infiltration rate, runoff develops rapidly, with ponding time controlled by soil hydraulic properties and initial moisture conditions. Consequently, infiltration rates vary considerably in time and space, even within a single soil type. Numerical models developed to estimate water partitioning are therefore sensitive to the choice of spatial and temporal resolution (Assouline and Mualem 2002; Huang et al. 2019). Due to data availability and computational demand, land surface models use approaches that overcome these limitations but may oversimplify the process (Anwar et al. 2019; Vereecken et al. 2019). These large-scale models (> 10 km grid size) often produce runoff, and consequently infiltration, only when rainfall rates exceed soil saturated hydraulic conductivity, limiting the role of ponding dynamics and relying only on saturation deficits to simulate runoff generation (Anwar et al. 2019; Crow et al. 2018; Grogan et al. 2022; Vereecken et al. 2019). Understanding how these approaches and associated scales influence water partitioning and the resulting spatial and temporal variability of runoff and streamflow is therefore crucial (Liu et al. 2019).

Here, we use the parsimonious, process-based hydrological model, DRYP (Quichimbo et al. 2021) to understand the influence of different spatial and temporal resolutions on water balance partitioning. DRYP is designed to capture the processes and water balance fluxes and stores of a dryland basin. We used combinations of three different model grid sizes (300 m, 1, and 5 km) and three model time steps (15 min, 1 h, and 1 day) to quantify how fluxes and water storage changes vary. This work expands on previous assessments of DRYP at 300 m resolution and 1 h time steps (Quichimbo et al. 2021) by not only examining how the scale influences modelled water partitioning but also by investigating the sensitivity of different infiltration equations to the spatial and temporal resolution. We use datasets from the semi-arid Walnut Gulch Experimental Watershed (WGEW), in SE Arizona, USA, where long-term, high-resolution information (e.g., precipitation, streamflow, soil moisture) is available to evaluate the performance of the model at various combinations of spatial and temporal resolutions. This analysis will allow us to identify the appropriate spatial and temporal resolutions that effectively capture the hydrological processes and the water balance for a dryland basin. This identification of appropriate resolutions can then be used to inform other applications of DRYP

10991085, 2026, 10, Downloaded from https://onlinelibrary.wiley.com/doi/10.1002/hyp.70733 by NICE, National Institute for Health and Care Excellence, Wiley Online Library on [16/10/2026]. See the Terms and Conditions (https://onlinelibrary.wiley.com/terms-and-conditions) on Wiley Online Library for rules of use; OA articles are governed by the applicable Creative Commons License

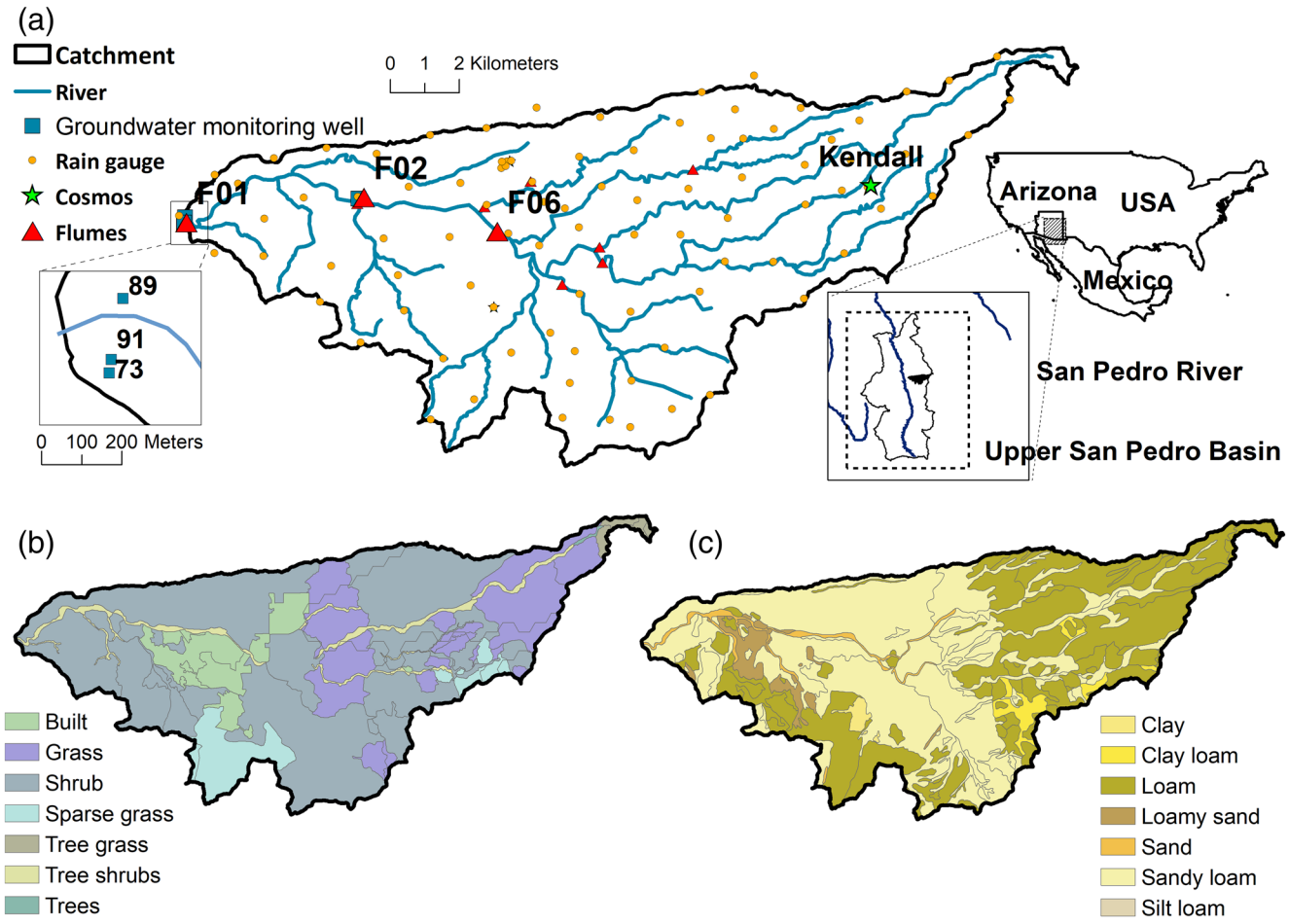


FIGURE 1 | (a) Geographic location of Walnut Gulch Experimental Watershed and location of monitoring stations, (b) land cover, and (c) soil spatial distribution over the basin.

(and potentially other dryland models) whether they are in smaller or larger basins or even at regional scales, independent from considerations of computational efficiency or resolution of available global datasets.

2 | Methods

2.1 | Walnut Gulch Experimental Watershed

The Walnut Gulch Experimental Watershed (WGEW), Arizona, USA (31°43′ N, 110°41′ W) (Figure 1) has a drainage area of ~149 km^2. It has a semi-arid climate with low annual rainfall averaging 312 $mm\,year^{-1}$ for the period 1956–2005, mostly delivered in the summer monsoon season (Goodrich et al. 2008). WGEW is mainly covered by shrubs and grass, with a high concentration of trees and shrubs along the channels (Skirvin et al. 2008). Hillslopes are dominated by gravelly and fine sandy loam soil texture types that generally have high values of hydraulic conductivity (Becker et al. 2018). Streambed sediments are composed of gravel and coarse sand with high values of porosity and infiltration rates (Singer and Michaelides 2014).

WGEW was chosen for this analysis because it has the highest spatial density of rain and streamflow gauges in a dryland basin worldwide and the data are resolved at high temporal resolution (Stone et al. 2008). The basin also has the longest global record of runoff in a semi-arid site covering the period 1954–2015. Historical records of event discharge at WGEW exist for this period at seven flumes along the main channel, numbered from F01 at the catchment outlet to F07 at the upstream end, and on seven tributaries. Event-based rainfall data exist for the same period at many of the 95 operational gauging stations across all WGEW at per minute and per rainfall event (Goodrich et al. 2008). These historical records of rainfall and discharge provide the opportunity to assess all key components of a model of dryland water balance and partitioning (Emmerich and Verdugo 2008; Goodrich et al. 2008; Keefer et al. 2008; Michaelides et al. 2018; Scott et al. 2015; Singer and Michaelides 2017; Stone et al. 2008). Within the basin there are also various stations that measure soil moisture and actual evapotranspiration (Emmerich and Verdugo 2008; Keefer et al. 2008), supporting a more robust evaluation of hydrological response. Additionally, although groundwater has been less comprehensively monitored at WGEW, patchy records of water table levels from three wells located close to the catchment outlet are available for assessing groundwater behaviour.

Runoff generation in WGEW is highly spatially and temporally variable and depends on rainfall intensity-duration, rainfall spatial location, antecedent soil moisture, and soil infiltration rates (Becker et al. 2018; Goodrich et al. 1997; Yatheendradas

10991085, 2026, 10, Downloaded from https://onlinelibrary.wiley.com/doi/10.1002/hyp.70733 by NICE, National Institute for Health and Care Excellence, Wiley Online Library on [16/10/2026]. See the Terms and Conditions (https://onlinelibrary.wiley.com/terms-and-conditions) on Wiley Online Library for rules of use; OA articles are governed by the applicable Creative Commons License

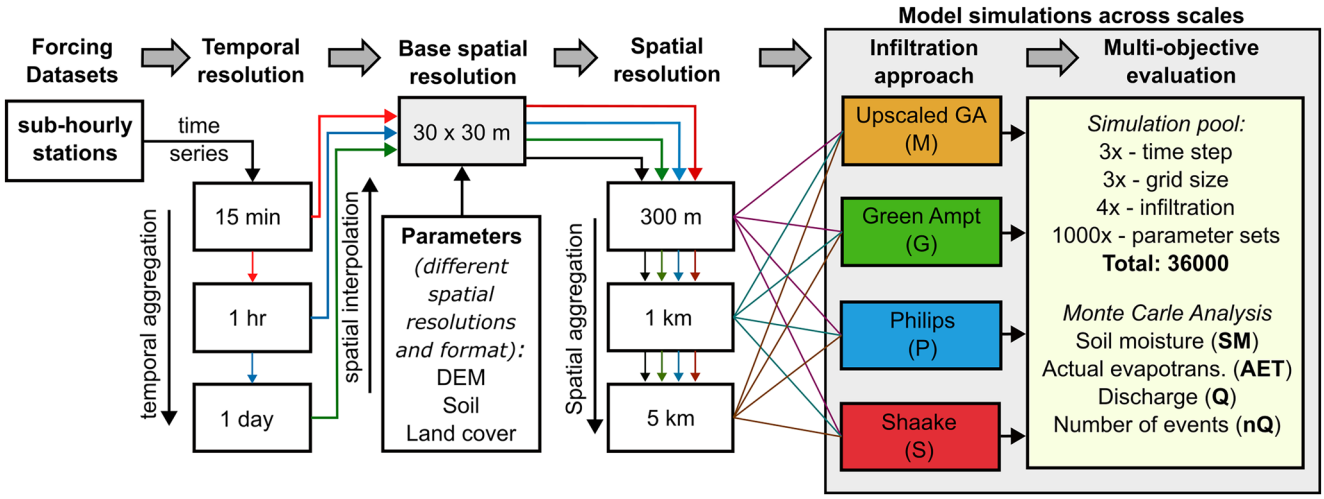


FIGURE 2 | Framework for multi-scale assessment of the effects of temporal and spatial scales on water partitioning (see Appendix A for differences among infiltration approaches).

et al. 2008). When runoff generation on the hillslope is sufficient in intensity and duration, it may accumulate as streamflow (flash floods) within ephemeral channels. Streamflow infiltrates into the channel bed as it moves downstream (e.g., (Keppel and Renard 1962; Singer and Michaelides 2014)), losing water as transmission losses, a component of which is thought to contribute focused groundwater recharge (Goodrich et al. 2013). The catchment is underlain by Tertiary and Quaternary alluvium sediments (Osterkamp 2008). The depth of the alluvial sediments is generally greater than 400 m, comprising clastic materials with a wide range of variation of particle size (clays to well-cemented boulders) (Osterkamp 2008). The water table is ~145 m below ground level (bgl) at flume F06 (Figure 1) and 50 m bgl close to the catchment outlet. A small, shallow, perched aquifer has also been delineated around flume F02 (Figure 1) (Goodrich et al. 2013).

2.2 | Parsimonious Model for DRYland Region Water Partitioning: DRYP

DRYP is a parsimonious distributed process-based, open-source hydrological model developed to quantify the water partitioning and flow paths in dryland regions (Quichimbo et al. 2021). The model consists of three main components: (i) a surface component that represents overland flow, streamflow and transmission losses, (ii) an unsaturated component for representing the soil and the riparian zone along streams, and (iii) a saturated flow component for representing groundwater flow. DRYP uses a single layer to represent the unsaturated zone. One of the novel characteristics of DRYP is that it represents the loss of water through the bed of an ephemeral stream, known as transmission losses, a key process in dryland regions. The model also includes four different alternative methods for partitioning precipitation into infiltration and runoff as a result of infiltration-excess, two point scale methods (i) Philip's infiltration (Philip 1987, 1957); (ii) a modified version of the Green & Ampt method (Green and Ampt 1911; Quichimbo et al. 2021); and two upscaled methods: (iii) the Upscaled Green & Ampt method (Craig et al. 2010); and (iv) the Schake approach (Schaake et al. 1996). Appendix A illustrates the differences in infiltration rates among the four approaches for a selected case study. The model also allows for easy adjustment of spatial and temporal resolutions. Further details of the model structure and functioning can be found in Quichimbo et al. (2021).

2.3 | Model Resolution Analysis Framework

The influence of model resolution within DRYP was evaluated by analysing model runs at various spatial and temporal resolutions. We did this by using three model grid sizes: 300 × 300 m, 1 × 1 km, and 5 × 5 km; and three model time steps: 15 min, 1 h and 1 day (Figures 2 and 3). The three grid sizes used in the analysis were chosen due to their potential suitability for use in large-scale model applications at regional and global scales (Bierkens et al. 2015; de Graaf et al. 2015; Wood et al. 2011). The selected resolutions were intended to represent distinct scales of model application rather than to provide a continuous assessment of resolution-dependent performance. Thus, the objective of this study is not to identify a specific spatial or temporal resolution threshold beyond which model performance deteriorates, but rather to investigate how changes in spatial and temporal resolution affect the representation and partitioning of water among hydrological fluxes and stores. In addition to varying grid size and time step, we also address how model resolution interacts with different infiltration equations. In dryland regions, the partitioning of precipitation into runoff and infiltration is one of the major sources of uncertainty on the quantification of the water balance. Therefore, we evaluated the effect of spatio-temporal resolution for four different in-built infiltration approaches listed above, which represent point-scale (Philips and Green & Ampt) and upscaled infiltration (Upscaled Green & Ampt and Schaake) methods to rainfall partitioning. Model simulations include 36 permutations of the three grid sizes, the three time-steps, and the four infiltration approaches (Figure 2).

10991085, 2026, 10, Downloaded from https://onlinelibrary.wiley.com/doi/10.1002/hyp.70733 by NICE, National Institute for Health and Care Excellence, Wiley Online Library on [16/10/2026]. See the Terms and Conditions (https://onlinelibrary.wiley.com/terms-and-conditions) on Wiley Online Library for rules of use; OA articles are governed by the applicable Creative Commons License

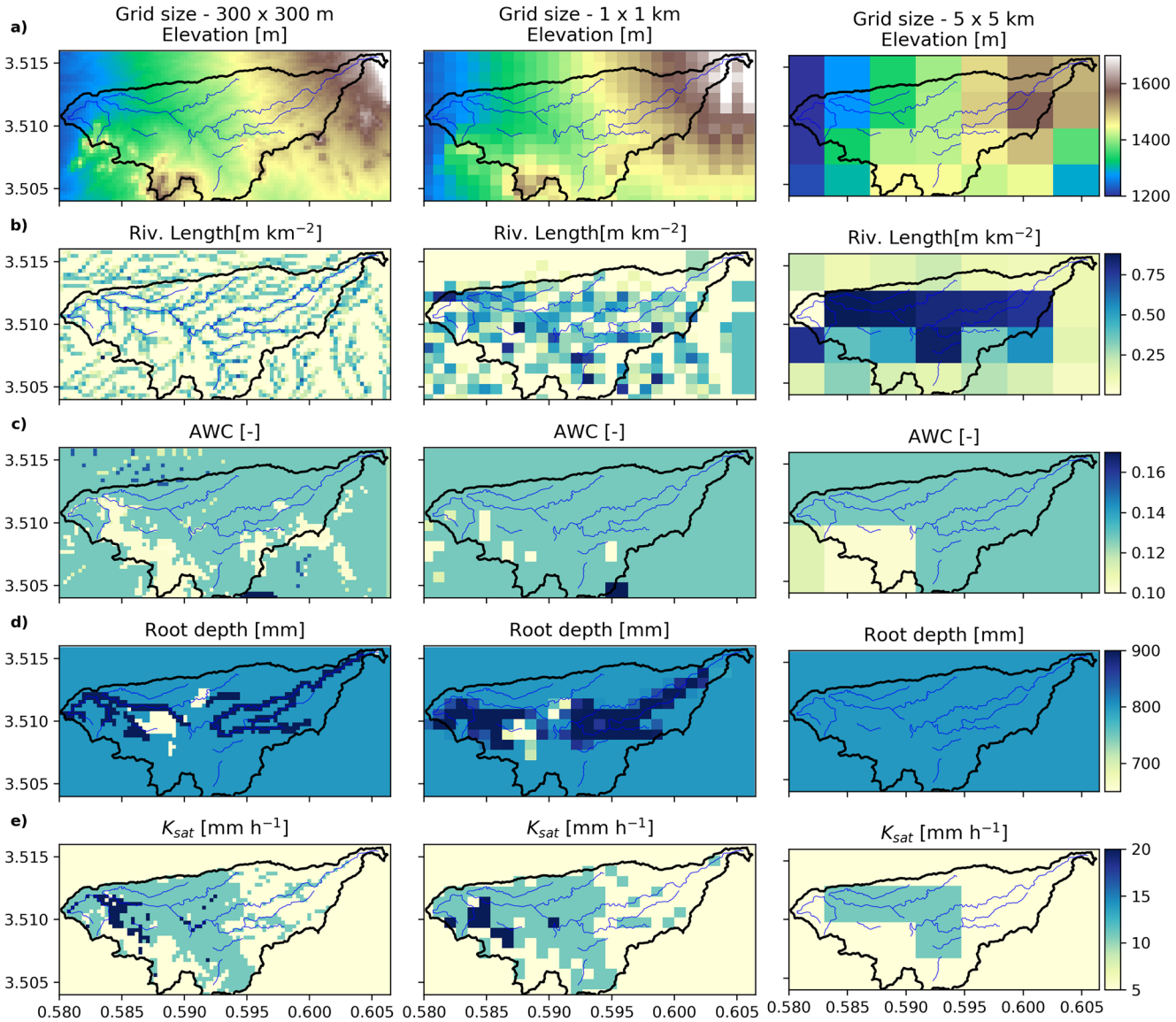


FIGURE 3 | (a) Topography, (b) river length, and soil hydraulic characteristics: (c) available water content (AWC), (d) rooting depth, and (e) K_{sat} saturated hydraulic conductivity for the three different grid scales (300 m, 1, 5 km). Values in square brackets are units and values in parenthesis are grid size, solid black line represent the WGEW, and solid blue lines represent streams. Length units of x and y axis are in 1000 km.

2.3.1 | Model Parameterisation for WGEW at Different Resolutions

A digital elevation model (DEM) of WGEW with a spatial resolution of 30 × 30 m was obtained from Shuttle Radar Topography Mission (SRTM) 1 Arc-Second Global map (available at https://earthexplorer.usgs.gov, last access: 15 May 2025). The DEM was aggregated by averaging cells into the three different grid sizes specified above (Figure 3a). Spatial distribution of soil texture and soil land cover were obtained from https://www.tucson.ars.ag.gov/dap/ as polygon files and were converted into model grid inputs by using the value of the feature with the largest percent of the pixel area.

Streams were delineated from the 30-m DEM by defining a minimal drainage area threshold of 0.65 km^2, which corresponds to the medium stream network resolution specified in Heilman et al. (2008). Stream lengths were estimated by aggregating the 30 × 30 m stream cells relevant to the various model grid sizes used (Figure 3b). Detailed information about channel width is not available for the basin, so a value of 10 m was used based on average point measurement available at locations close to flumes (Miller et al. 2000; Smith et al. 1982). Channel widths were kept constant across all spatial resolutions to reduce potential bias resulting from the spatial aggregation method. This approach isolates the effect of spatial resolution on the representation of channel length and drainage structure, while avoiding additional resolution-dependent changes in channel width.

Based on the soil texture (see Figure 1), baseline hydraulic properties required for modelling were obtained from Rawls et al. (1982) and Clapp and Hornberger (1978) (Table S1). Clapp and Hornberger (1978) water retention parameters were considered owing to their simplicity and their potential transferability to regions where only coarse information is available. Values of field capacity and wilting point required to estimate

10991085, 2026, 10, Downloaded from https://onlinelibrary.wiley.com/doi/10.1002/hyp.70733 by NICE, National Institute for Health and Care Excellence, Wiley Online Library on [16/10/2026]. See the Terms and Conditions (https://onlinelibrary.wiley.com/terms-and-conditions) on Wiley Online Library for rules of use; OA articles are governed by the applicable Creative Commons License

the total available water (Figure 2c) were estimated by using the Brooks and Corey (1964) pedotransfer function to obtain the water retention curve, assuming matric potentials of −33 kPa and −1500 kPa, respectively, following the FAO guidelines (Walker 1989). Soil rooting depth was estimated according to land cover and using reference values for different types of vegetation from Lesschen et al. (2004) (Figure 3e).

2.3.2 | Forcing Datasets

Point measurements of rainfall were obtained from 98 rainfall stations available on https://www.tucson.ars.ag.gov/dap/ (last accessed 01/10/2021). Rainfall data were processed in two main stages. First, the time series of rainfall at each gauging location (Figure 1) was aggregated to the specified model time step (e.g., 15 min, 60, and 1 day) and then spatially interpolated to a 30 × 30 m grid size using a Natural Neighbour algorithm (Park et al. 2006). In the second stage, the temporally gridded rainfall was spatially aggregated to the resolution of the spatial domains considered for the analysis (300 m, 1, and 5 km) (Figure 2).

Rain gauges at WGEW are regularly calibrated (Goodrich et al. 2008), so we assume that the measurements have low uncertainty. However, interpolation and aggregation processes are likely to introduce error to the rainfall estimation. Spatial and temporal aggregation of rainfall have been shown to significantly affect the performance of hydrological models (Faurès et al. 1995; Goodrich et al. 1997, 1994; Yatheendradas et al. 2008). Errors up to 130% and 90% in runoff volume and peak discharge, respectively, have been reported at WGEW by previous studies due to spatial aggregation in rainfall for specific events (Lopes 1996). Therefore, we anticipate that aggregation of input rainfall will contribute a source of uncertainty in the model outputs, which will be considered within our evaluation via performance indices (see next section).

We used an hourly potential evapotranspiration (hPET) dataset (Singer et al. 2021), which estimates PET via a Penman Monteith approach (Allen et al. 1998) based on climate variables from the ERA5-Land reanalysis dataset (Hersbach et al. 2020). hPET has a spatial resolution of ~9 km at the equator and is publicly available at https://data.bris.ac.uk/data/dataset/qb8ujazzda0s2aykkv0oq0ctp (last access: 10 December 2023). This dataset was used to force DRYP with evaporative demand required to close the water balance at its high native resolution, supporting greater potential to accurately drive hydrological and land surface models (Albergel et al. 2018; Alfieri et al. 2020; Tarek et al. 2020). The coarser spatial resolution of hPET is expected to have very limited impact on the water balance since the spatial variation of PET within the model domain is considerably lower than precipitation. Additionally, the higher rates of PET in relation to precipitation, common in water limited environment, will also further minimize the effect of the coarser resolution.

2.3.3 | Evaluation Data for WGEW

2.3.3.1 | Actual Evapotranspiration. Data from the AmeriFlux eddy covariance flux tower site, Kendall Grassland (US-Wkg) located within WGEW, were used for model evaluation (Glenn et al. 2015; Scott 2010). Uncertainty of flux tower data is mainly attributed to instrumental and random errors and increases with flux magnitude (Richardson et al. 2006; Schmidt et al. 2012) with mean relative errors of ~5% with deviations of ±16% (Schmidt et al. 2012). Historical records of AmeriFlux data from mid-2006 to 2018 for model evaluation were downloaded from https://ameriflux.lbl.gov/sites/siteinfo/US-Wkg (last access: 20 July 2021).

2.3.3.2 | Soil Moisture Measurements. We used a cosmic-ray neutron sensor located within the WGEW catchment to evaluate the model performance against soil moisture (Figure 1) (Zreda et al. 2012). Data from the Kendall station were corrected for atmospheric pressure (Zreda et al. 2012), atmospheric vapour pressure (Rosolem et al. 2013), and variation in background intensity by using the Cosmic-Ray Sensor PYthon tool (Power et al. 2021). A detailed description of parameters and calibration procedure is provided in Desilets et al. (2010). Records from mid-2010 to 2018 were used for model evaluation. These publicly available data were downloaded from http://cosmos.hwr.arizona.edu/Probes/StationDat/010/index.php (last access: 20 July 2021).

2.3.3.3 | Runoff Measurements. Runoff at 11 small watersheds and the catchment outlet is measured regularly by critical and subcritical depth flumes. However, only three main flumes (F01, F02, and F06) located along the main channel were selected for this analysis (Figure 1) because they span the length of the channel well enough to be captured under all spatial resolutions considered here. The upstream contributing areas reported for these three flumes are 149, 119, and 95 km^2 for F01, F02, and F06, respectively (Stone et al. 2008). Flumes at WGEW have been designed to capture the high variability of flow; therefore, the reliability and accuracy of the measurements exhibit low uncertainty (Stone et al. 2008). However, the distribution of runoff over the surface after a rainfall event in the model is highly dependent on the intersection between the local expression of the rainfall and topographic characteristics of the catchment; thus, spatial aggregation of the DEM to coarser scales is expected to impact model results.

2.3.3.4 | Groundwater Observations. Available groundwater measurements at WGEW are sparse in both time and space, limiting a comprehensive evaluation of surface-groundwater processes at the study site. However, a mixture of daily and hourly groundwater level records for two periods, mid-1999–2004 and mid-2017–mid-2018, from three wells located close to the catchment outlet (Figure 1) were available and used for the evaluation of the model's focused recharge component. It should be noted that the water table at WGEW is well below the channel elevation over most of the catchment, so groundwater contributions to baseflow are rare.

2.4 | Model Calibration and Identification of Behavioural Models

The DRYP model has seven free parameters of which four are contained within the surface component (Quichimbo et al. 2021), which is the focus of the calibration here: (1)

10991085, 2026, 10, Downloaded from https://onlinelibrary.wiley.com/doi/10.1002/hyp.70733 by NICE, National Institute for Health and Care Excellence, Wiley Online Library on [16/10/2026]. See the Terms and Conditions (https://onlinelibrary.wiley.com/terms-and-conditions) on Wiley Online Library for rules of use; OA articles are governed by the applicable Creative Commons License

saturated hydraulic conductivity (K_{sat}), (2) rooting depth (D_{root}), (3) channel hydraulic conductivity (K_{ch}), (4) recession time of streamflow or the average time that flow remains in each grid cell (T). We obtained initial values for the first three of these parameters from soils data (Table S1), whereas we set the initial value of T to 1 m/s, based on mean annual values reported elsewhere (Allen et al. 2018). We recognize there may be high uncertainty in these values (indeed the original parameter values did not result in good model performance), so we defined hypothetical ranges for each these parameters based on multiplicative factors of the original parameter values (kK_{sat}, kD_{root}, kK_{ch}, kT) (Table S2). This method of parameter estimation maintains the original spatial distribution of parameter values. Selected prior parameter ranges were chosen based on their sensitivity evaluated in a preliminary analysis (Quichimbo et al. 2021). Then we use these parameter ranges in a Monte Carlo framework to identify the best fit values for each parameter using the Generalized Likelihood Uncertainty Estimation (GLUE) framework (Beven and Binley 1992), which also allows us to identify behavioural models (those which match the observed values of streamflow, actual evapotranspiration, and soil moisture).

The GLUE framework considers that, owing to the uncertainty of the input data and the limitations of boundary conditions, there are multiple sets of parameters that can produce acceptable (i.e., behavioural) simulations. To determine which simulations were considered behavioural, we used a combination of three different 'goodness of fit' indexes (Krause et al. 2005): the Nash–Sutcliffe Efficiency (NSE) (Nash and Sutcliffe 1970), percent bias (PBIAS), and the coefficient of determination (R^2) defined as follows:

$$\mathrm{NSE} = 1 - \frac{\sum_{i=1}^{n}\left(O_i - S_i\right)^2}{\sum_{i=1}^{n}\left(O_i - \bar{O}\right)^2} \tag{1}$$

$$\mathrm{PBIAS}(\%) = 100 \cdot \frac{\sum_{i=1}^{n} O_i - \sum_{i=1}^{n} S_i}{\sum_{i=1}^{n} O_i} \tag{2}$$

$$R^2 = \frac{\left(n \cdot \sum_{i=1}^{n} O_i \cdot S_i - \sum_{i=1}^{n} O_i \cdot \sum_{i=1}^{n} S_i\right)^2}{\left[n \cdot \sum_{i=1}^{n} O_i^2 - \left(\sum_{i=1}^{n} O_i\right)^2\right]\left[n \cdot \sum_{i=1}^{n} S_i^2 - \left(\sum_{i=1}^{n} S_i\right)^2\right]} \tag{3}$$

where O represents observations, $\bar{O}$ is the arithmetic mean of observations, S represents simulated values, and n is the number of observations available.

For a simulation to be deemed behavioural, we defined a set of thresholds for each variable evaluated depending on the uncertainty of the observations. For streamflow, high uncertainty is expected due to the spatial aggregation of model parameters and variables. Hence, values of NSE greater than or equal to 0.50 and PBIAS less than or equal to 20% were considered as behavioural simulations. It should be noted that while 20% of simulated streamflow seems like a large tolerance at face value, it only represents less than 1% of the total water budget of the study area. NSE index ranges between 1 (perfect fit) and -∞, with values of 0 meaning that model estimations are not better than the mean value of observations; thus, values greater than 0.5 indicate good agreement between model and observations (K. J. Beven 2004; Krause et al. 2005). For the number of events, values of R^2 greater than 0.5 were considered behavioural, whereas for soil moisture and actual evapotranspiration, values of NSE greater than 0.5 were specified. In order to combine these measures into a single performance metric, models which did not meet these conditions were assigned a value of zero, whereas for any remaining models the indices were scaled between 0 and 1. For NSE and R^2 values, the highest value was assigned 1, whereas for PBIAS, the lowest value was assigned a value of 1.

The combined performance measure was then calculated as the product of all indexes considered in the analysis:

$$p_i = \left(\prod_{k=1,2,6} NS_k^* \cdot PBIAS_k^* \cdot R_k^{2*}\right)^{1/m} \tag{4}$$

where p is the combined performance measure for the i-th parameter set, the * indicates scaled values, k represents the variable, and m represents the number of variables considered in the analysis.

For soil moisture, a direct comparison between observation and simulations is not possible, given that the soil moisture observations are depth-specific (Franz et al. 2012), whereas the model uses a single soil layer. Therefore, given the lack of information to characterize the distribution of soil moisture across soil depth (Albergel et al. 2008; Wagner et al. 1999), a simple approach to scale soil moisture values was used for the evaluation (Quichimbo et al. 2021):

$$O^* = O^{\alpha} + S_{min} \tag{5}$$

where * indicates the scaled value, and α is estimated by:

$$\alpha = \frac{\log\left|S_{max} - S_{min}\right|}{\log\left|O_{max} - O_{min}\right|} \tag{6}$$

The period between 01/01/2007 and 01/01/2018 was used as the calibration period to overlap with the period of flux tower observations and streamflow data, but soil moisture was only evaluated for the period of available data, 01/10/2010–01/01/2018. A warm-up period of 1 year, prior to the evaluation period, was used to reduce the influence of the model initial conditions on model outputs.

Note that we use the entire period 2007–2018 for evaluation of model outputs under different spatial and temporal resolutions, as well as infiltration equations, even though much of this period was also used for model calibration. This longer period corresponds to the time domain after a switch over to digital rainfall gauges in WGEW (Goodrich et al. 2008). Given the high variability of streamflow in this dryland basin, a large sample of gauged observations is required to represent the hydrological responses to climate forcing (Zoccatelli et al. 2019). Furthermore, this approach is reasonable since our goal here is to evaluate model outputs under different resolutions to ascertain impacts on the water balance, rather than to predict hydrological responses to conditions not yet experienced in the basin.

10991085, 2026, 10, Downloaded from https://onlinelibrary.wiley.com/doi/10.1002/hyp.70733 by NICE, National Institute for Health and Care Excellence, Wiley Online Library on [16/10/2026]. See the Terms and Conditions (https://onlinelibrary.wiley.com/terms-and-conditions) on Wiley Online Library for rules of use; OA articles are governed by the applicable Creative Commons License

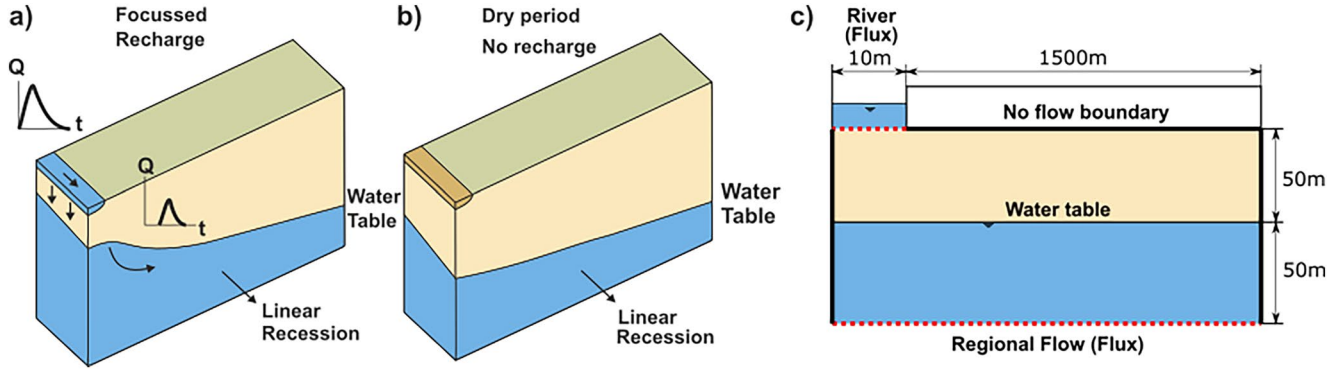


FIGURE 4 | Conceptual model for evaluation of estimated focused recharge, and a diagram for model setup. (a) water table mound during recharge event, (b) water table linear recession after the recharge has occurred, and (c) groundwater model setup and boundary conditions.

The spatial aggregation of topography at the selected grid sizes is also likely to influence the flow direction within the model domain. Changes in flow direction affect the contributing area of subbasins, and this in turn may affect the temporal and spatial distribution of runoff over the entire model domain and particularly at flume locations. It is expected that models at high spatial resolution (300 m) will be less affected by the redistribution of contributing areas, whereas coarser models, particularly the 5-km grid size, will have large discrepancies in relation to the finer resolution. Therefore, the use of all three flumes along the main channel for the selection of behavioural models is only considered when the contributing area of these flumes varies up to 20% from reported values in (Stone et al. 2008). If one flume does not meet this requirement, only one flume is used in the selection of behavioural models.

A total of 36 000 (Figure 2) simulations were performed in the calibration process: that is, 1000 sets of parameters drawn from a uniform distribution for each of the 36 combinations of the four infiltration approaches (Philip's, Schaake, upscaled GA, and modified GA), three timesteps (15, 60 min, and 24 h), and three grid sizes (300 m, 1 and 5 km) (Table S2). This allows us to isolate the secular effects of either spatial resolution, temporal resolution, or infiltration approach on the water balance.

2.5 | Evaluation of Focused Recharge From Behavioural Models

Once we obtained behavioural models, we sought to evaluate the realism of the focused recharge generated by these models, which is a key component of the partitioning of water in this dryland basin. This evaluation occurred outside the GLUE framework, given the limited spatial extent of available groundwater data in comparison with the spatial and temporal scale of the models, and the fact that the deep water table at WGEW means that stream-aquifer interactions are unidirectional, where water generally only moves from the surface to the subsurface aquifer (Quichimbo et al. 2020). Thus, the evaluation of the modelled recharge was performed separately from the catchment model using a bespoke 1D transect model by taking the total recharge output from the basin-scale model at the location of flume F01 and using this output to drive 1D simulations of water table evolution. The goal is not to capture the dynamics of the water table across the entire model domain, but rather to assess the magnitude and timing of simulated focused groundwater recharge and its influence on water-table dynamics at locations where groundwater-level observations are available (see Figure 1a). This step is important to better constrain aquifer recharge via transmission losses below the channels.

Accordingly, a 1D DRYP model was set up to capture the small-scale influence of focused recharge on the water table near the ephemeral stream channel. Focused recharge is expected to produce a local mounding of the water table that will lead to an initially steep recession due to transverse groundwater flow perpendicular to the channel. This steeper recession will eventually be attenuated and will often transition to a more linear shape governed by the regional groundwater recession, which expresses the ratio of long-term recharge to specific yield of the aquifer (Cuthbert 2014; Cuthbert et al. 2016), This is a common process in dryland regions where the recharge is sporadic, and this latter linear recession has also been reported by Goodrich et al. (2013) at WGEW.

A schematic representation of the model and the geometrical characteristics of the model domain is shown in Figure 4. The model domain consisted of 1×100 active grid nodes and one layer. Grid size elements were specified as 15×15 m. Values of specific yield, Sy [–], were assumed to vary between 7% and 9% according to hydrogeological reports of aquifers with similar geological characteristics, that is, cemented conglomerates, located in areas close to WGEW (Pool and Schmidt 1997; USBR 1977). Flux boundary conditions were specified at the channel cells and at the bottom of the model domain, whereas no-flow boundary conditions were specified for the rest of the model domain (Figure 3). The flux boundary at channel cells represents the focused recharge and was obtained from the catchment model outputs after calibrations. Focused recharge from the closest stream cells to the monitoring well was used to define input flow rates to the aquifer. The flux boundary at the bottom was used to represent the longitudinal recession. Flow rates for the long-term longitudinally driven linear recession were calculated to emulate the observed head changes over the period between 2002 and 2004, for which groundwater monitoring data is available. This period corresponds to water table changes at which groundwater mounding, due

10991085, 2026, 10, Downloaded from https://onlinelibrary.wiley.com/doi/10.1002/hyp.70733 by NICE, National Institute for Health and Care Excellence, Wiley Online Library on [16/10/2026]. See the Terms and Conditions (https://onlinelibrary.wiley.com/terms-and-conditions) on Wiley Online Library for rules of use; OA articles are governed by the applicable Creative Commons License

to the input pulse, dissipated (see Figure 6 in the Results section). Considering the range of variation of aquifer specific yield, *Sy*, the flux boundary condition varies from 0.00007 to 0.00009 $m^3\ d^{-1}$. Initial conditions for the water table were specified as 50 m deep from the model top elevation, which corresponds to the mean annual water table depth registered by the monitoring wells at WGEW.

2.6 | Assessing the Water Balance Over Different Temporal and Spatial Resolutions

Finally, we evaluated how the water balance varied for different spatial and temporal model resolutions and for different infiltration equations. To do this, we collated mean annual values of modelled fluxes and stores for the entire basin from all behavioural models for each permutation of resolution and infiltration equation into ensembles, which can be summarized for each flux/store as a distribution. This allowed us to directly compare ensembles of model outputs across resolutions.

A grid-by-grid comparison was not performed because spatial aggregation of topography substantially alters surface-flow pathways and, consequently, the contributing areas within the basin. This effect is particularly important at the 5-km grid size, where aggregation can considerably modify the contributing areas to the flumes and therefore influence which models are classified as behavioural. Consequently, grid cells at different spatial resolutions do not necessarily represent equivalent hydrological units, making direct grid-by-grid comparisons difficult to interpret. We therefore focused on basin-scale water-balance partitioning and model performance as a consistent basis for evaluating the effects of spatial and temporal resolution.

3 | Results

3.1 | Capturing Water Balance Dynamics for the 'Best' Calibrated Models

We first verify the best behavioural model against observed data to see how well the calibrated models perform in capturing key components of the water balance. We identified the best overall combination of spatial and temporal resolution and infiltration approach was the Philips equation at 300 m and 1 h (P300m60min). The discussion below provides a detailed evaluation of all behavioural models for P300m60min as a demonstration of how well DRYP captures the dynamics of different components of the WGEW water balance. It is also worth noting here that the best model from this analysis matches previous simulations of the same basin (Quichimbo et al. 2021).

In general, modelled soil moisture, actual evapotranspiration, and discharge at the catchment outlet show a good agreement in terms of dynamics in response to input precipitation with their corresponding observed/proxy variable (Figure 5). A comparison between simulated and measured soil moisture data, after scaling (see Section 2.4), shows good agreement with NSE values above 0.60 (Section 3.2, Figure 6b). Indicating that the best model well captures the dynamics of the soil moisture over the evaluation period (Figure 5b). However, we acknowledge that the transformation of observed values is likely to introduce some artefacts since it is unable to capture the variation of the effective depth of saturation of the measured soil moisture (Dimitrova-Petrova et al. 2020; Franz et al. 2013, 2012). This effective depth of saturation is greater (~33 cm) for low values of soil moisture (5%) and shallower (~16 cm) at higher values of soil moisture (65%). This may explain the discrepancies between simulated and observed peak values.

The best model also well captures (NSE ~0.60) the overall temporal variation in evapotranspiration (Figure 5c). However, discrepancies are observed at peak events in 2016 and 2017 where AET is overpredicted, which may in part stem from uncertainties in the data. Discrepancies between flux towers and simulated AET up to 15% for 1 year have been reported for grassland vegetation in previous studies (Scott 2010; Twine et al. 2000), where such errors are mainly attributed to the uncertainty in rainfall and latent heat flux measurements (Scott 2010). This may also be attributed to the lack of a dynamic vegetation component in the existing models (Warter et al. 2020), as the crop coefficient factor in the water balance calculation is currently assumed constant over the entire simulation period.

The best model also well captures the monthly temporal variability of runoff at the three main flumes (F01, F02, and F06) along the main channel with values of NSE above 0.60 (Figure 5d–f). This includes simulating the correct number of streamflow events ($R^2 > 0.75$) for the evaluation period. However, the performance of the model varies along the channel, for example, high peak values at flume F06 are underpredicted (e.g., 2008, and 2012), whereas, at downstream flumes for the same events the model shows a better fit. The number of streamflow events is underpredicted at flumes F02 and F01, however this does not seem to impact the overall volume of streamflow events. The underestimation of runoff during wet years may be attributed to high intensity rainfall events that increase the hydraulic conductivity of the soil as a result of surface soil crust removal, which consequently increases the infiltration rate (Becker et al. 2018), an effect not currently included in DRYP. Discrepancies are also attributed to the redistribution of drainage areas due to the spatial aggregation of the topography as indicated above. Changes in catchment areas for different spatial aggregations affects the timing and the volume of water at each stream cell and consequently the overall production of runoff.

Regarding focused groundwater recharge below the streambed, simulated changes in the water table depth from the 1D model driven by outputs from the basin-scale model agree with water table observations, particularly for the last period of available data, mid 2017 to late 2018 (Figure 6). This suggests that behavioural basin-scale models are generating realistic values of total recharge. Therefore, the total estimated recharge for these models can be used as reference values for comparison across scales and infiltration approaches used in this analysis. For the year 2001, when there was no large streamflow event captured by the model, recharge is underestimated and consequently the extent of the groundwater mounding is also underestimated.

10991085, 2026, 10, Downloaded from https://onlinelibrary.wiley.com/doi/10.1002/hyp.70733 by NICE, National Institute for Health and Care Excellence, Wiley Online Library on [16/10/2026]. See the Terms and Conditions (https://onlinelibrary.wiley.com/terms-and-conditions) on Wiley Online Library for rules of use; OA articles are governed by the applicable Creative Commons License

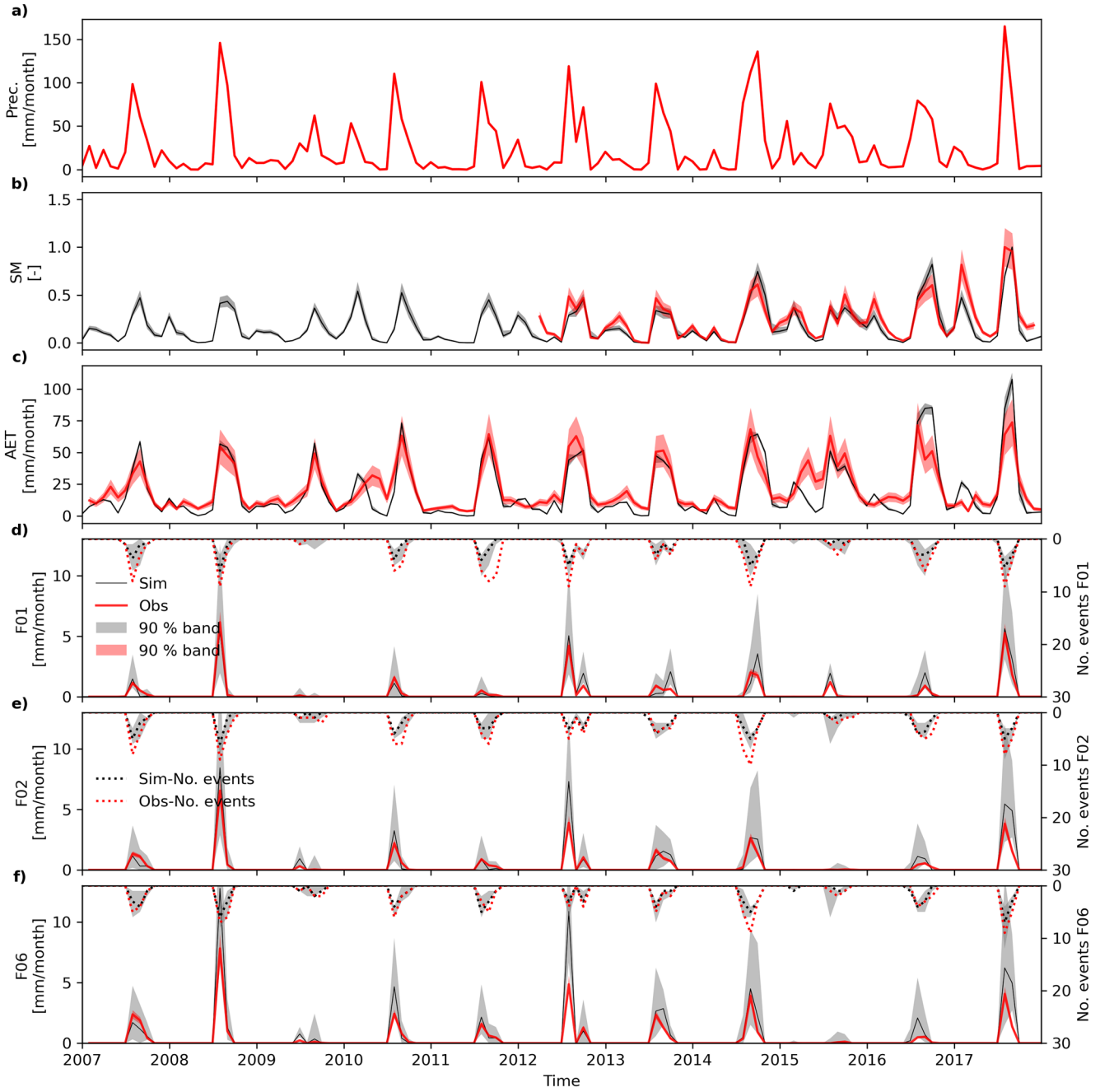


FIGURE 5 | Comparison between observed (red) and simulated (P300m60min) (black) values of monthly temporal variations of (a) precipitation, (b) soil moisture at cosmos Kendall location, (c) actual evapotranspiration at Kendall, (d) streamflow at flume F01, (e) streamflow at flume F02, and (f) streamflow at flume F06. See Figure 1 for station locations.

However, the overall linear recession rate illustrates that the amount of water recharging the aquifer between 2004 and 2017 is simulated well as the water table matches the observation at the end of the simulated period.

3.2 | Analysis of Overall Model Performance and Uncertainty

Below we examine all behavioural model simulations for each permutation of spatial and temporal resolution and infiltration equation. Section 2.6 showed that the grid resolution of the DEM affected the size of the contributing subbasin areas. At the catchment outlet, flume F01, the contributing area for the three model grid sizes (300 m, 1, and 5 km) showed variations of 2%, 8.5%, and −2%, respectively, when compared to the reference values (see Section 2.3.3). At flume F02, variations in subbasin area were estimated to be 3%, 13%, and −2% for the 300 m, 1, and 5 km model grid sizes, respectively; and for flume F06, variations in contributing areas were 4%, −5%, and −42% for model grid sizes of 300 m, 1, and 5 km, respectively. This variation in contributing area to each streamflow flume precluded the evaluation of the 5-km grid resolution models at the three flumes, and so 5-km simulations were only evaluated at the catchment outlet (F01).

10991085, 2026, 10, Downloaded from https://onlinelibrary.wiley.com/doi/10.1002/hyp.70733 by NICE, National Institute for Health and Care Excellence, Wiley Online Library on [16/10/2026]. See the Terms and Conditions (https://onlinelibrary.wiley.com/terms-and-conditions) on Wiley Online Library for rules of use; OA articles are governed by the applicable Creative Commons License

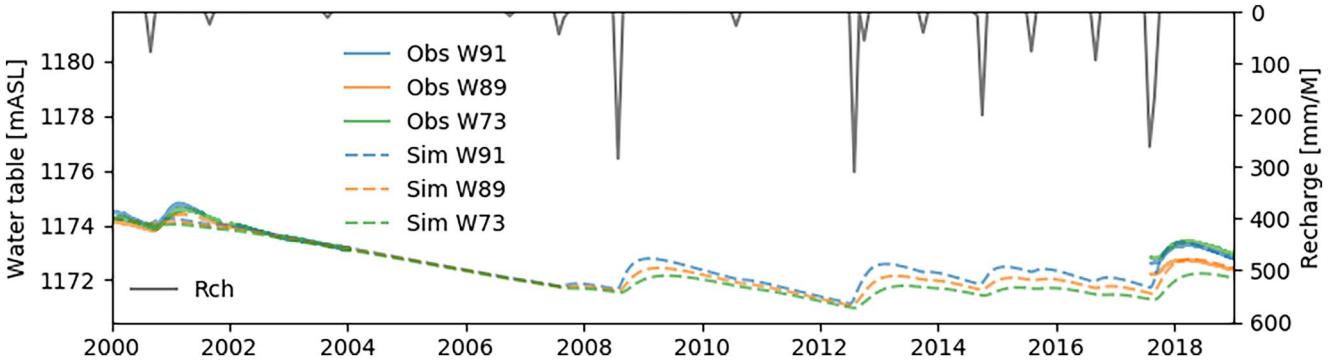


FIGURE 6 | Temporal variation of groundwater recharge at the river cell of the flume F01 (see Figure 1) from the best basin scale model (Section 3.2) (top x-axis), and comparison of simulated and observed values of water table elevation; locations of monitoring wells are shown in Figure 1. Simulated water table elevations were obtained from the 1D groundwater model (see Section 2.5).

Figure 7a show the overall performance (p-value) based on evaluation at all flumes, soil moisture, and AET, of each permutation of resolution and infiltration equation plotted against the number of behavioural models for that permutation. Only the best models for each grid resolution and time step (and infiltration method) are plotted. All models are labelled by the infiltration model followed by the grid resolution and the time step at the end (e.g., Model-1 km-60 min). The infiltration model is specified as follows: M for modified Green and Ampt, P for Philip's model, S for Schaake, and G for the Green and Ampt model (see Figure 2). Models at 5 km resolution are not included in Figure 7a because they could not be evaluated at all flumes. All Schaake infiltration models failed to reach the threshold specified for evaluation at all 3 flumes mainly due to their inability to capture the number of runoff events. However, the S-300m-15min models were included in the analysis, despite failing the threshold for the number events, to compare their performance in relation to the rest of models.

Overall, model performance varies highly with spatio-temporal resolution and infiltration equation. Although we do not show the non-behavioural models, such models were mostly rejected due to higher absolute values of streamflow PBIAS and low correlation on the number of simulated runoff events. Most behavioural models came from the Philip's infiltration equation at 300-m grid size and 15-min time step. However, the best overall model uses the same Philip's infiltration approach but at the spatial and temporal resolution of 300 m and 60 min. It is important to note that for both Philips (P) and modified GA models (M), the 15-min models perform better than the 60-min time step, suggesting that high temporal resolution is needed to best capture the runoff response to input rainfall.

The best models show good ability to represent both soil moisture and AET with NSE values for both exceeding 0.55 (Figure 7b). Soil moisture does not show a strong sensitivity to the temporal resolution and infiltration method, as values of NSE show a small range of variation (between 0.64 and 0.67) for behavioural models at 15-min and 60-min resolutions. At the 300 m spatial resolution, values of actual evapotranspiration show variations in response to changes in temporal resolution with values of NSE falling between 0.55 and 0.64 for behavioural models. However, the NSE increases to its highest value (~0.67) for the 1-km and 60-min spatial and temporal resolution respectively. Thus, the model P-1 km-60 min is the best model for representing the dynamics of both the soil moisture (NSE ~0.70) and actual evapotranspiration at WGEW. The S-300 m-15 min model also shows good performance with similar values of NSE for both AET and soil moisture, in comparison to valid models (Figure 7b).

Figure 7c shows the model performance in relation to the number of streamflow events of flumes F01 against flume F06. Models at the spatial resolution of 5 km have also been added to the figure in order to evaluate temporal variability of the model at coarser scales. Again, the scale of the model as well as the infiltration method greatly affect model performance. In general, results show a high R^2 (> 0.6) for all valid models, with the P-300 m-60 min showing the best performance at both flumes. For the 5-km grid size, the best models are the ones that use the Philip's infiltration equation at 15-min and 60-min time steps. Models with a time step of 24 h also appear to have good performance, despite the coarser temporal and spatial resolution. High values of R^2 suggest good ability of the model to capture the development of ephemeral streams at a monthly timescale, regardless of their magnitude. However, the good model performance is also due to the strong correlation between streamflow events and rainfall events. These results suggest that the number of events is not sensitive to the performance of the model or the spatial and temporal scale. However, the number of events is very sensitive to the infiltration method, which ultimately resulted in the rejection of all Shaake models, as mentioned above.

Figure 7d–f shows the estimated NSE against PBIAS in streamflow for the three flumes. Results for models at 5-km grid size were also added; however, they were only evaluated at flume F01 because of discrepancies in catchment contributing areas at upstream flumes (see Section 2.6). In general, all behavioural models capture the dynamics of flow (NSE > 0.5) but have lower skill in capturing the overall mass fluxes, particularly at flume F01, where we see high values of PBIAS. Again, the best model (P-300m-15min) has the highest NSE (~0.95) and a PBIAS of 12%. P-300m-60min and M-300m-60min models have slightly lower performance in relation to the best model (NSE = 0.90 and 0.86 respectively) and a PBIAS of 12% for both models, which indicates their skill. There is a

10991085, 2026, 10, Downloaded from https://onlinelibrary.wiley.com/doi/10.1002/hyp.70733 by NICE, National Institute for Health and Care Excellence, Wiley Online Library on [16/10/2026]. See the Terms and Conditions (https://onlinelibrary.wiley.com/terms-and-conditions) on Wiley Online Library for rules of use; OA articles are governed by the applicable Creative Commons License

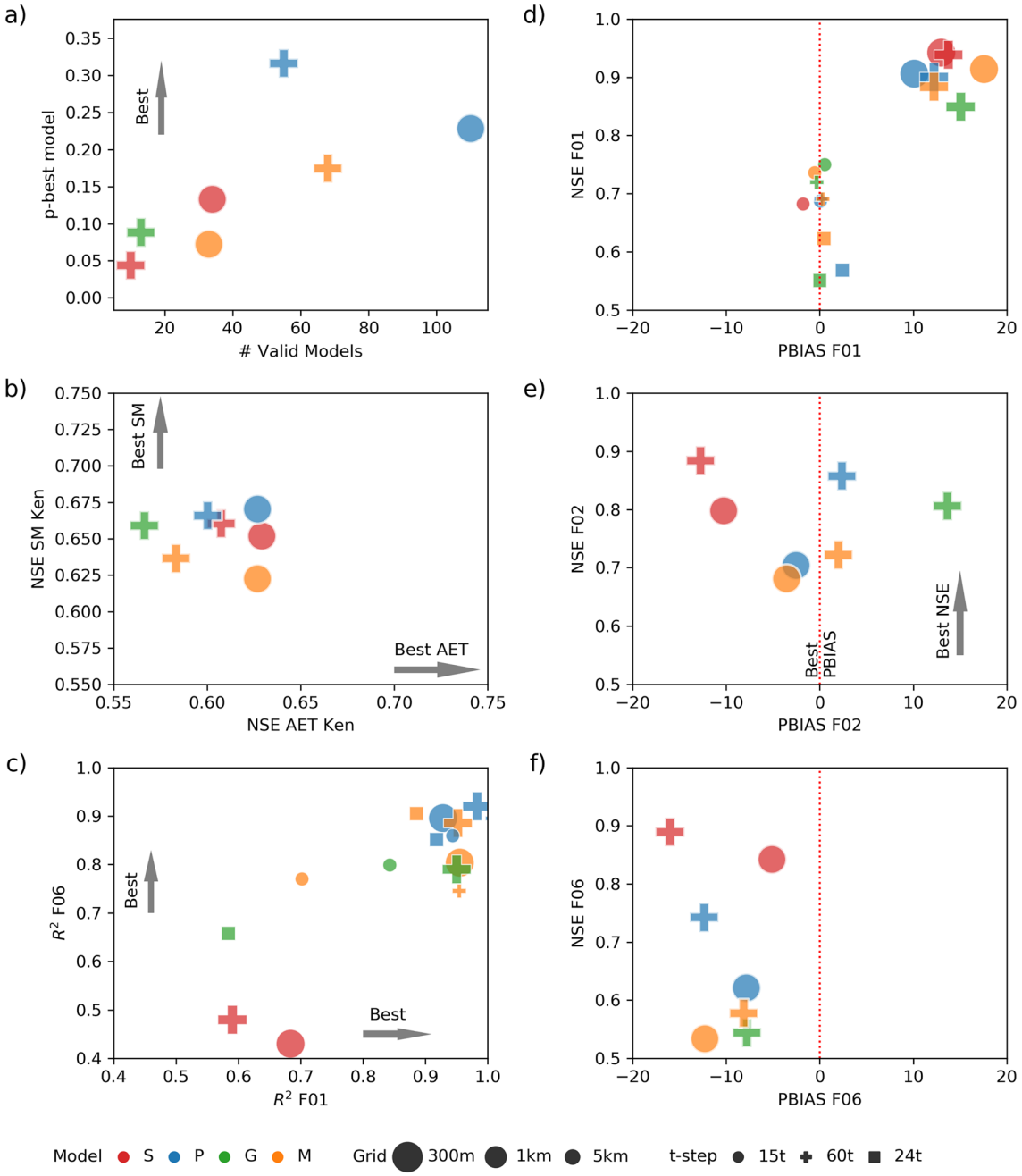


FIGURE 7 | Indices estimated for the best behavioural models selected according to the combined performance metric 'p' (Equation 4) based on the evaluation of flumes F01, F02 and F05, and soil moisture and AET at Kendall. (a) Estimated 'p' against the number of valid models resulted from the Monte Carlo analysis for different grid size, time-step, and infiltration approach. (b) NSE for the soil moisture (SM) estimated at the Kendall location against NSE of the evapotranspiration at Kendall location. (c) R^2 of flumes F06 against F01. Panels (d–f) represent the NSE against the PBIAS for the three flumes located along the main channel, flume F01, F02 and F06. Results at 5-km grid size were evaluated only at flume F01. Models using different infiltration methods are represented as P = Philip's, S = Schaake, G = upscaled Green and Ampt, and M = modified Green and Ampt. Marker size represents model spatial resolution with the biggest size representing the highest resolution. Models at 5-km grid size do not consider the evapotranspiration on the evaluation.

notable decline in model performance for discharge with distance upstream of the catchment outlet for all models, suggesting a challenge for capturing the streamflow dynamics at the upstream flumes (Figure 7e,f). The mass balance represented by PBIAS switches from positive to negative values at the farthest upstream flume (F06), which results in overestimation of streamflow, whereas at the catchment outlet streamflow is underestimated.

3.2.1 | Variability of Model Parameters

For all behavioural models ($p > 0$) for all permutations of spatial and temporal resolution and infiltration equation, the distributions of parameters that greatly impact model performance are shown in Figure 8. Recall that k represents a scaling factor applied to the initial estimated parameter values (moving all values up or down) to maintain the spatial distribution of model

10991085, 2026, 10, Downloaded from https://onlinelibrary.wiley.com/doi/10.1002/hyp.70733 by NICE, National Institute for Health and Care Excellence, Wiley Online Library on [16/10/2026]. See the Terms and Conditions (https://onlinelibrary.wiley.com/terms-and-conditions) on Wiley Online Library for rules of use; OA articles are governed by the applicable Creative Commons License

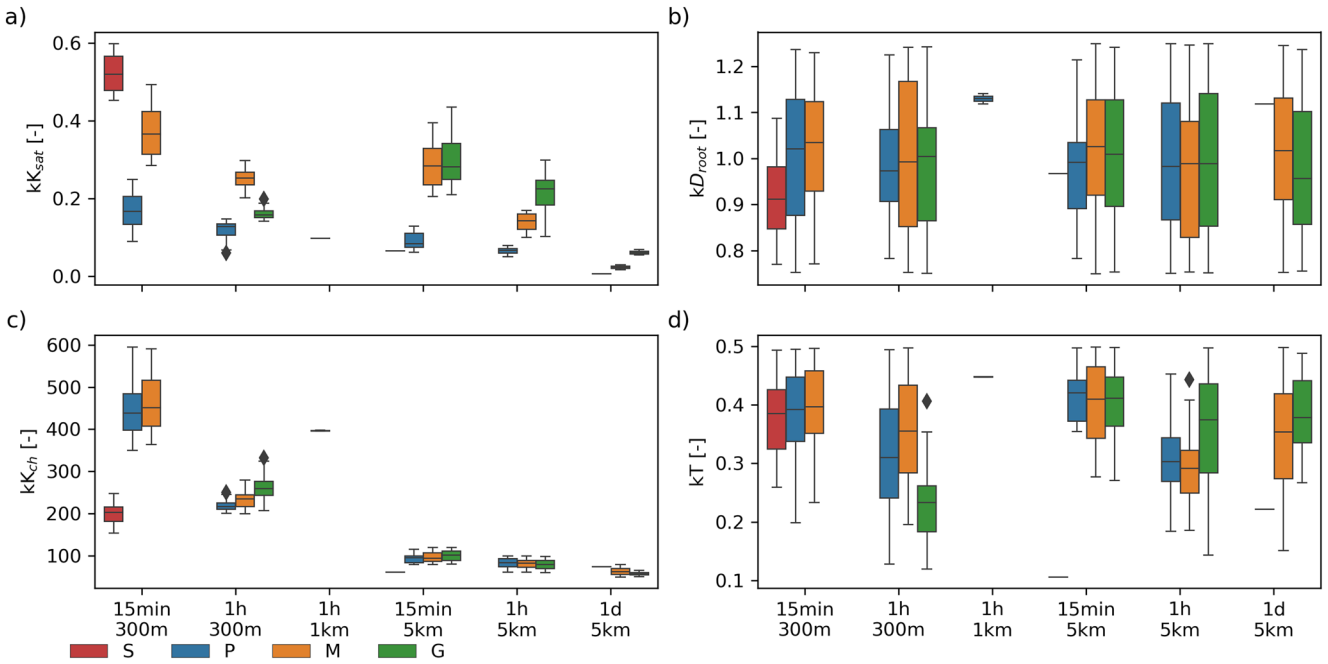


FIGURE 8 | Distribution of parameter factors (a) kK_{sat}, (b) kD_{root}, (c) kK_{ch}, and (d) kT for behavioural simulations based on evaluation at flumes F01, F02 and F06, and soil moisture and AET at Kendall. Results at the 5-km grid size were evaluated only at flume F01. Models using different infiltration methods are represented as P = Philip's, S = Schaake, G = upscaled Green and Ampt, and M = modified Green and Ampt. Models at 5-km grid size are not considered in the evaluation the evapotranspiration.

parameters. A narrow distribution of a parameter suggests that model results are quite sensitive to that model parameter. Results show a narrow distribution for parameters that control the production of runoff, kK_{sat}, (Figure 8a) and the volume of transmission losses, kK_{ch}, (Figure 8c), whereas the parameter that controls the flow routing, kT, has a broader distribution (Figure 8d).

Figure 8a shows that values of kK_{sat} depend on the infiltration method and the model spatial and temporal resolution. In general, when the spatial or temporal resolution of the models increases (becomes coarser), the magnitude of the K_{sat} must be reduced in order to allow the model to capture the production of runoff. This is expected because the peaks of rainfall events are flattened with aggregation of both spatial and temporal resolution. This results in low infiltration rates that are required to reduce the amount of water entering the soil in order to produce the expected runoff. Thus, for the best model, using the Philip's infiltration equation, the multiplicative factor of hydraulic conductivity (kK_{sat}) must be reduced from 0.2 for the 300 m–15 min models to 0.01 for the 5 km–24 h models. It can also be seen that values of kK_{sat} for the modified Green and Ampt model are higher than the rest of the models for larger spatial and temporal resolutions. The differences in magnitude of K_{sat} values for different model structures mean that infiltration rates at the beginning of the precipitation event play an important role in the partitioning of precipitation (see also Michaelides and Wilson 2007). Higher values of K_{sat} mean that models produce less infiltration at the onset of the precipitation event than models with lower K_{sat} values.

The distribution of the factor controlling rooting depth (kD_{root}) varies between 0.85 and 1.12, with mean values ~1.0 (Figure 8b) across different scales and infiltration methods. These results suggest that the model outputs are less sensitive to the rooting depth than K_{sat}. Less variation in D_{root} means that the storage in the unsaturated zone is almost similar across all models. This factor is important for diffuse recharge across the landscape, as large values in D_{root} combined with low rainfall rates will prevent the production of recharge as the water storage capacity of the soil increases.

For channels, the factor controlling the hydraulic conductivity (kK_{ch}) also needs to be reduced at coarser temporal and spatial scales (Figure 8c). However, this calibrated factor exhibits less variation between infiltration methods compared to K_{sat}. This means that similar rates of water infiltration through the streambed are expected. In contrast, the parameter that controls channel storage shows low sensitivity to temporal and spatial scales (Figure 8d). Higher values of kT signify higher velocity rates along the channel. In summary, the choice of infiltration method mainly influences the production of runoff via the K_{sat} parameter and good simulations of discharge at the catchment outlet, are affected by the channel infiltration parameter (K_{ch}). Therefore, these two infiltration parameters (on hillslopes and in the channel) play an important role in the performance of the model.

3.3 | Impact of Spatial and Temporal Model Resolution and Infiltration Approach on the Water Balance Components

Results of the water balance obtained from the behavioural models are shown in Figure 9, which presents distributions of each component of the water balance as a percentage of the input precipitation. Results from all behavioural models across all

10991085, 2026, 10, Downloaded from https://onlinelibrary.wiley.com/doi/10.1002/hyp.70733 by NICE, National Institute for Health and Care Excellence, Wiley Online Library on [16/10/2026]. See the Terms and Conditions (https://onlinelibrary.wiley.com/terms-and-conditions) on Wiley Online Library for rules of use; OA articles are governed by the applicable Creative Commons License

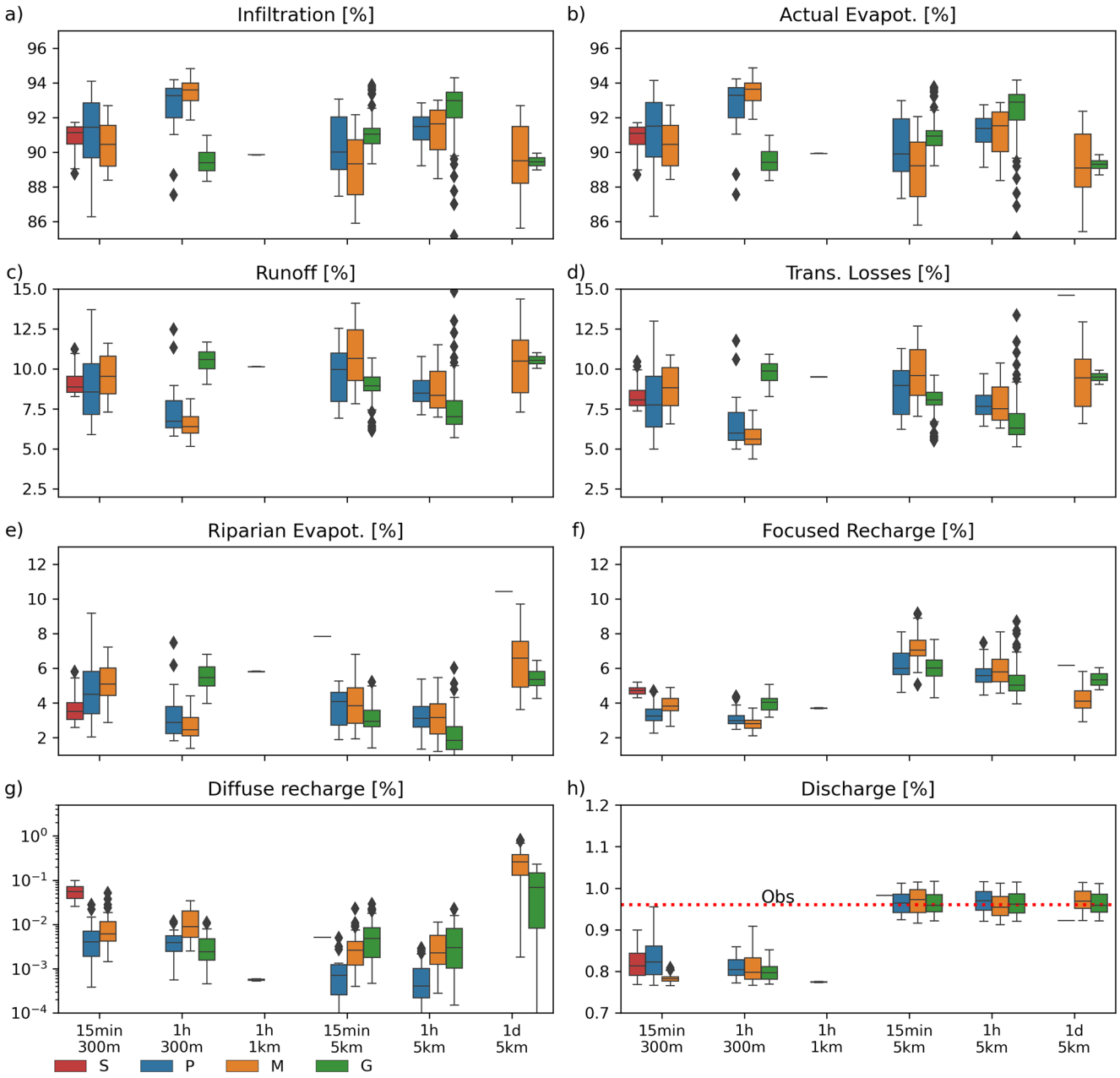


FIGURE 9 | Flux distribution as a percentage of precipitation for behavioural models based on the evaluation at flumes F01, F02 and F06, and soil moisture and AET at Kendall. Results at 5 km grid size were evaluated only at flume F01.

temporal and spatial scales and infiltration equations show that infiltration is the highest flux representing up to 95% of the input precipitation (Figure 9a). The M-300m-60min shows the highest mean values of infiltration (~93%). Mean infiltration values do not show a great variation with model structure (91%–94%), even though calibrated infiltration parameters (K_{sat}) show high variations for different infiltration equations. The high range in K_{sat} (Figure 8a) reflects that this parameter largely controls the ratio of precipitation and infiltration regardless of the choice of the infiltration method employed in DRYP. Actual evaporation is the second largest flux of the WGEW water balance (85%–94%), and one of the main sources of water losses within the basin. Actual evapotranspiration consumes almost all the infiltrated water (Figure 9b) due to high rates of potential evapotranspiration typical of this semi-arid environment.

For all behavioural models, the production of overland flow varies from 5% to 25%, with most infiltration methods showing a mean value of runoff of 8%–11% (Figure 9c). However, runoff is greatly reduced by transmission losses, which represent around 3%–15% (Figure 9d). Also, models at the 5-km grid resolution and 24-h time step show the highest values of diffuse recharge (Figure 9g), which is attributed to the few high rainfall events due to temporal aggregation of intense rainfall that creates a drizzle effect (Kipkemoi et al. 2021), along with high initial infiltration rates at the initiation of precipitation events that allow water to percolate through the soil.

For the best model– the P-300m-60min—the simulated transmission losses are ~5% of the input rainfall and are low in comparison to other models (mean values ~8%–10% of rainfall). The

10991085, 2026, 10, Downloaded from https://onlinelibrary.wiley.com/doi/10.1002/hyp.70733 by NICE, National Institute for Health and Care Excellence, Wiley Online Library on [16/10/2026]. See the Terms and Conditions (https://onlinelibrary.wiley.com/terms-and-conditions) on Wiley Online Library for rules of use; OA articles are governed by the applicable Creative Commons License

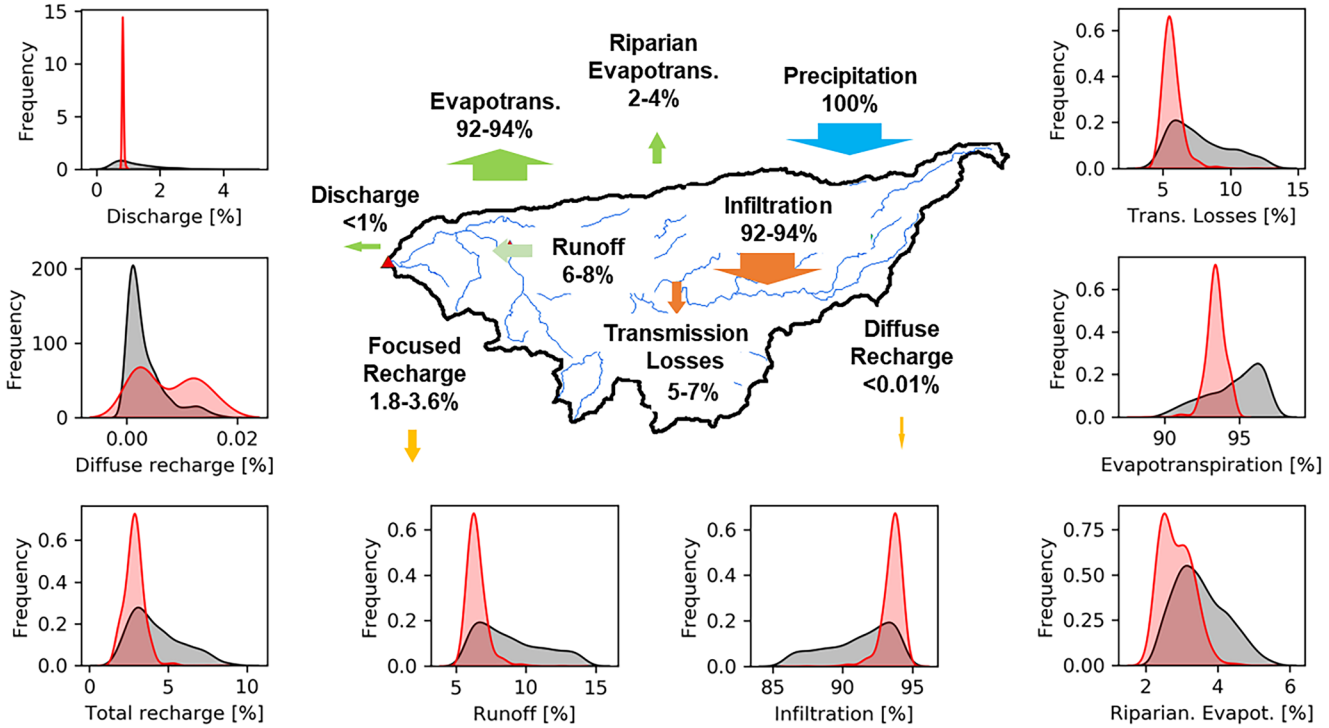


FIGURE 10 | Schematic representation of the water balance components of the WGEW based on the best model: Philips-300m-60min. Arrow scale and direction depend on the magnitude of the components and direction indicates inflow/outflow. Grey shaded areas represent the entire population of model simulations, whereas red shaded areas represent the distribution of behavioural models only.

low percentage of transmission losses of the modified Green-Ampt results from high volumes of infiltration (Figure 9c) due to the high K_{sat} values, which consequently results in low runoff production (Figure 9f). To compensate for the low production of runoff and to get a better estimation of discharge at the outlet for this permutation, the parameters K_{ch} had to also be reduced by kK_{ch} (Figure 8b). The rest of the models work in a similar way; the production of streamflow is generally regulated by the downward flux of transmission losses.

Finally, the overall water balance for the WGEW from the behavioural simulation of the best model configuration (P-300m-1h) is presented in Figure 10, details of the model selection are described in Section 2. The figure also shows the distribution of all simulations to illustrate the impact that uncalibrated parameters may have in the water balance components. The uncertainty of uncalibrated parameters may be considerably high; therefore, transferring those parameters to other basins may result in considerable high uncertainty. It is also noted that the estimation of water fluxes and environmental states in the basin coincides with previous studies (e.g., (Quichimbo et al. 2021; Renard 1970; Renard et al. 2008)). Infiltration and evapotranspiration are the main fluxes (> 92% of the precipitation), with evapotranspiration consuming almost all infiltrated water typical of a dryland environment. Focused recharge represents between 1.8% and 3.6% of the total input rainfall, whereas diffuse recharge is below 0.01%.

4 | Discussion

We have presented a comprehensive analysis of the impact of the spatio-temporal resolution (and infiltration method) of the hydrological model (DRYP) on the variability of the various fluxes of the water balance in a dryland basin. Below we focus the discussion on: (i) the performance of DRYP in characterizing water fluxes for dryland regions including model skill at capturing surface-groundwater interactions; (ii) the sensitivity of water partitioning to spatial and temporal model resolutions; (iii) the methodological advance of model parameter calibration that achieves good results while remaining faithful to the spatial distribution of input datasets; and (iv) the implications of this research for making progress in simulating the water balance in dryland (and/or humid) areas at regional and global scales.

4.1 | Model Performance in Accurately Representing Hydrological Fluxes in Dryland Regions

We found that behavioural models at high spatial resolution (e.g., 300 m) and at sub-daily time scales showed the most skill in representing streamflow, actual evapotranspiration and soil moisture. At these high resolutions, DRYP also produced highly accurate results of groundwater recharge, particularly focused recharge and their influence on water table fluctuations (Figure 6). This is a key feature of this modelling system designed to capture interactions between surface water and groundwater, forced by climate and opens up many possibilities for using the model under different climate forcings to understand the potential impacts on groundwater storage changes (IPCC6 2021). Notably, we also found that behavioural models at 1-km spatial resolution and at 1-h temporal resolution had skill in characterizing the various components of the water balance. Additionally, we found that the infiltration approach plays an

10991085, 2026, 10, Downloaded from https://onlinelibrary.wiley.com/doi/10.1002/hyp.70733 by NICE, National Institute for Health and Care Excellence, Wiley Online Library on [16/10/2026]. See the Terms and Conditions (https://onlinelibrary.wiley.com/terms-and-conditions) on Wiley Online Library for rules of use; OA articles are governed by the applicable Creative Commons License

important role in the model performance due to its influence on rainfall-runoff partitioning, such that completely different results may arise for different water balance components based only on differences in the infiltration approach (Figure 9). This has important implications for the modelling community, as models may need more constrains to better represent the water balance. Overall, we found that the Philips approach resulted in the best model performance.

Our analysis points to the importance of streamflow as a key calibration dataset for selecting behavioural models (Figure 5), as obtaining good results for streamflow led to a substantial reduction in the number of behavioural models (Figure 10). Ultimately, it is challenging for any rainfall-runoff model to generate accurate streamflow time series (K. J. Beven 2004), and this challenge grows markedly in dryland regions, where the hydrologic response to rainfall is very nonlinear (Faurès et al. 1995; Goodrich et al. 1997). Our results also indicate the great impact of rainfall partitioning between runoff and infiltration in the water balance, which in addition to the flow routing approach can lead to great uncertainty in model outputs. However, for WGEW it is important to consider that the proportion of runoff (e.g., Hortonian overland flow on hillslopes) in relation to other components of water balance is small, with values as a percentage of input precipitation of less than 1%. This factor, in combination with the uncertainty due to the spatial aggregation of the DEM supports a set of low thresholds chosen for the evaluation indices. For example, a PBIAS threshold of 20% can yield accurate results for this dryland study area (Figure 7). Additionally, our modelling analysis revealed the challenge of using a simple implicit flow routing approach to capture the strong spatial and temporal variation of streamflow in such a dynamic basin (Cortés-Salazar et al. 2023), even if it still captures the dynamics of the main water balance components (Figure 5).

4.2 | Sensitivity of Water Partitioning to Model Resolution and Infiltration Method

Our analysis revealed strong variability in water partitioning at different spatial and temporal resolutions. Models at 300-m and 5-km resolutions result in an increase of infiltration as the temporal resolution decreases from 15 min to 1 h because forcing datasets (rainfall and PET) are aggregated in time. This temporal aggregation dampens the intensity and disproportionately affects the small precipitation events. In fact, dampening these small precipitation events results in total infiltration of rainfall events, a result that is consistent with prior work done in a 1D framework (Kipkemoi et al. 2021). This effect is propagated through all flux components in order to close the water balance with the observations. Thus, runoff, transmission losses, riparian evaporation, and recharge all become reduced, whereas actual evaporation increases to compensate for the surplus of infiltration generated at low temporal resolutions.

The behavioural model at 5-km spatial resolution shows a decrease in average values of infiltration for the 1-day temporal resolution. This contrasts with the increase in infiltration when the temporal resolution decreases from 15 min to 1 h. At the coarser spatial and temporal resolutions (5 km and 1 day), where the aggregation greatly impacts the high and low precipitation events, the model balances the overall amount of water required for producing enough runoff from peak and low events through low infiltration rates. There is a trade-off between runoff and transmission losses as the high runoff produced by low infiltration rates on slopes is then reduced by transmission losses in channels. The production of runoff is mainly controlled by K_{sat}, which shows the lowest calibrated values at 5-km resolution (Figure 8a), and therefore causes water to quickly accumulate in the rooting zone, which in turn results in higher values of diffuse recharge (Figure 9g). The comparison of model fluxes across different scales shows that diffuse recharge may be overestimated at coarse temporal scales (daily time scales). Therefore, high temporal resolutions may be more appropriate to represent diffuse recharge regardless of spatial resolution. Similarly, to capture the main characteristics of the streamflow and focussed recharge components of the water balance in DRYP, a high temporal resolution (< 1 day) of rainfall forcing is required. In contrast, soil moisture and AET are much less sensitive to larger temporal aggregations of rainfall forcing above 1 day. This behaviour highlights the challenge of representing the water balance in dryland regions where the spatial and temporal variability of precipitation is high (Singer and Michaelides 2017).

We also observed that there is more variability of water fluxes between different infiltration approaches than for different spatial and temporal resolutions (Figure 9). This variability means that different infiltration approaches compensate water fluxes within the model domain in order to match the observed datasets. In fact, we found that high infiltration rates at the onset of the rainfall event are critical in the development and distribution of runoff events, which ultimately affect the water balance outputs of the model. This process is of critical importance because infiltration excess is the main mechanism of runoff generation in dryland environments (Dunkerley 2018; Pilgrim et al. 1988).

4.3 | Calibration of Model Parameters

The model parameter sensitivity analysis showed that soil and channel saturated hydraulic conductivity, across scales and infiltration methods, are the most sensitive parameters for DRYP to have skill in representing streamflow. In general, behavioural models required smaller values of saturated hydraulic conductivity for longer time steps and/or larger grid sizes (Figure 8). This is consistent with the expected effect of the spatial and temporal aggregation of forcing datasets. The spatial distribution of model parameters was kept constant over the entire model domain, as only a multiplicative factor was applied for calibration. This condition assumes that input soil datasets are highly accurate in capturing the soil spatial distribution, which can be a challenge to parameterize from regional and global datasets (Dai, Shangguan, et al. 2019; Dai, Xin, et al. 2019; Montzka et al. 2017; Pelletier et al. 2016). Changing the spatial distribution of parameters could significantly improve the model's performance, albeit in an uncertain way that may ignore observed metrics of environmental variables. Additionally, calibrating all parameters at each pixel independently would considerably increase the number of simulations required for calibration.

10991085, 2026, 10, Downloaded from https://onlinelibrary.wiley.com/doi/10.1002/hyp.70733 by NICE, National Institute for Health and Care Excellence, Wiley Online Library on [16/10/2026]. See the Terms and Conditions (https://onlinelibrary.wiley.com/terms-and-conditions) on Wiley Online Library for rules of use; OA articles are governed by the applicable Creative Commons License

The calibration also shows that it is harder to generate behavioural models as the spatial resolution decreases because the range of variation of sensitive model parameters narrows. This has great implications for the transferability of model parameters to ungauged basins or for model application at regional or global scales since the uncertainty of estimated fluxes can be considerably high.

Additionally, our modelling analysis points to trade-offs between runoff generation and transmission losses that lead to equifinality in simulating flow at a particular flow gauge. Having more measurements along the channel helps to constrain streamflow within the model domain and therefore to accurately represent transmission losses along channels. Therefore, estimates of transmission losses are highly uncertain without additional observational constraints from multiple flow gauges along the channel (e.g., 5 km resolution models were calibrated only to one flume). This indicates an advantage of using DRYP within other data-sparse dryland regions of the world, since its simplicity and efficiency enables a full exploration of the range of uncertainty, which would be impossible with a more complex model.

Our evaluation also showed that considering observations of soil moisture and evapotranspiration in conjunction with streamflow in the selection of behavioural models reduces the uncertainty of the estimation of most of the water balance components. However, the uncertainty in measured soil moisture and estimated AET may be larger than streamflow in absolute terms in dryland settings. Hence, the relative accuracy of the streamflow estimation may still be very uncertain, for example as measured as PBIAS (Figure 7). The analysis also showed that good prediction of the number of flow events is easier to achieve for a wide range of infiltration methods, as well as for different spatial and temporal resolutions than is required to obtain accurate volumetric discharge estimates. Thus, while the number of runoff events may not be a good metric for the overall water balance, it may be very useful for predicting the probability of wetting events that may have local significance for dryland water resources and hazards (Larned et al. 2010; Leigh and Datry 2017; Steward et al. 2012).

4.4 | Implications for Land Surface Modelling at Regional and Global Scales

Most hydrological models capture the interactions between the climate and the hydrological responses of fluxes, but they completely ignore the surface-groundwater interactions that impact underlying aquifer storage. Here, by using a 1D groundwater model we have showed that the best model provides values of groundwater recharge that accurately reproduce the water table fluctuations at the WGEW (Wallace and Renard 1967). Thus, the analysis highlights the skill of DRYP to produce accurate estimates of focused recharge due to transmission losses at higher spatial and temporal resolutions (e.g., 300 m–1 h, Figure 6). Focused recharge was found to be the main mechanism of groundwater recharge in the WGEW, which is consistent with the current understanding of recharge processes in dryland environments (Cuthbert et al. 2016; Pilgrim et al. 1988; Quichimbo et al. 2023; Schreiner-McGraw et al. 2019; Schreiner-McGraw and Vivoni 2018; Seddon et al. 2021). This skill makes DRYP a powerful tool that can enhance the quantification of the water balance in drylands and reduce the uncertainties surrounding the sensitivity of groundwater to climate change variability (IPCC6 2021).

Finally, the performance of behavioural models, particularly at the 1-km scale, reveals that a relatively simple model, such as DRYP, has the potential to accurately represent water partitioning on a large scale- both regionally and globally. Here, we showed that the long-term values of water fluxes, and particularly focused recharge, for the 1-km resolution simulations vary within the range of the 300-m resolution simulations (Figure 9f). This agreement between the two spatial resolutions is crucial for understanding the complex dynamics of water distribution in dryland environments, which are currently poorly represented in large-scale hydrological or land surface models. Furthermore, we found good performance for the 1-km spatial resolution, in combination with a 1-h temporal resolution. This combination allows for the representation of the development of flowing ephemeral streams within DRYP, a process which generally requires high computational demand because it necessitates complex numerical solutions, making its application at regional and global scales unfeasible (Goodrich et al. 2012; Lahmers et al. 2019; Schreiner-McGraw et al. 2019; Schreiner-McGraw and Vivoni 2018; Woolhiser 1989; Zoccatelli et al. 2019). Thus, DRYP shows important promise for overcoming the limitation of current models for potential application in simulating the dynamics of the water balance in response to climate for any dryland region of the world.

5 | Conclusions

In this paper, we analysed the influence of model temporal and spatial resolution and different infiltration methods on water partitioning and the overall water balance for a dryland basin. We used the parsimonious water partitioning dryland model (DRYP), which we calibrated separately for each of several permutations of spatial and temporal resolutions and (built-in) infiltration method, and evaluated the water balance outputs against observations of streamflow, soil moisture, evapotranspiration and groundwater level data from the semi-arid Walnut Gulch Experimental Watershed (Arizona, USA). We assessed the sensitivity of water partitioning by identifying behavioural simulations based on multi-parameter Monte-Carlo experiments evaluated against a range of objective performance metrics.

Overall, the analysis shows that high spatial resolution models (e.g., 300 m) at sub-daily temporal resolution show the best performance for representing streamflow, actual evapotranspiration and soil moisture. However, models at 1-km spatial resolution are also able to perform nearly as well at the 1-h temporal resolution. The infiltration approach also plays an important role in the model performance due to its influence on rainfall-runoff partitioning and the Philips approach was found to produce the best model performance.

Our analysis also revealed that the saturated hydraulic conductivity of the soil, K_{sat}, and the channel, K_{ch}, play a key role in model performance because they control the production of

10991085, 2026, 10, Downloaded from https://onlinelibrary.wiley.com/doi/10.1002/hyp.70733 by NICE, National Institute for Health and Care Excellence, Wiley Online Library on [16/10/2026]. See the Terms and Conditions (https://onlinelibrary.wiley.com/terms-and-conditions) on Wiley Online Library for rules of use; OA articles are governed by the applicable Creative Commons License

runoff and transmission losses. We found these parameters need to be reduced at coarser temporal and spatial resolutions.

For the WGEW, the modelled water balance components are consistent with previous studies (e.g., (Quichimbo et al. 2021; Renard 1970; Renard et al. 2008)), highlighting infiltration and evapotranspiration as the main fluxes (> 92% of the precipitation), with evapotranspiration consuming almost all infiltrated water. Focused recharge represents between 1.8% and 3.6% of the total input rainfall, whereas diffuse recharge is below 0.01%. Also, evapotranspiration from riparian zones greatly reduces the amount of transmission losses when it infiltrates into the alluvial sediments (by 40%–60%).

Finally, the analysis highlights the potential of a simple, parsimonious model to accurately represent all components of the water balance in dryland environments at coarser spatial resolution, for example, 1-km. This is important because it enhances our ability to accurately represent dryland hydrological processes at regional and global scales. Having this modelling capability provides the opportunity to enhancing our understanding of climate change variability in dryland environments which are typically underrepresented and sparsely gauged or monitored. Thus, this study paves the way for consideration of how larger scale hydrological models can improve their process representation in drylands.

Acknowledgements

Datasets were provided by the USDA-ARS Southwest Watershed Research Center. Funding for these datasets was provided by the United States Department of Agriculture, Agricultural Research Service. E. A. Quichimbo received financial support from the European Commission Horizon 2020 Postdoctoral Fellowships—Marie Skłodowska-Curie 640 ("HYDROAWARE AFRICA", grant no 101209082), UKRI-EPSRC-Strategic Impact Funding, and Cardiff University through a Vice Chancellor's Scholarship. Mark O. Cuthbert gratefully acknowledges funding for an Independent Research Fellowship from the UK Natural Environment Research Council (grant no. NE/P017819/1). Michael Bliss Singer has been supported by the U.S. National Science Foundation (grant nos. BCS-1660490 and EAR-1700555) and the U.S. Department of Defence's Strategic Environmental Research and Development Program (grant no. RC18-1006). Rafael Rosolem has been supported by the Natural Environment Research Council (NERC), under the MOSAIC Digital Environment Feasibility Study (grant no. NE/T005645/1), and by the International Atomic Energy Agency of the United Nations (IAEA/UN; project no. CRP D12014). Katerina Michaelides acknowledges support from a University of Bristol Research Fellowship and Leverhulme Research Fellowship (grant no. RF-2023-591\4). The team has been supported by the Global Challenges Research Fund (GCRF; "Impacts of Climate Change on the Water Balance in East African Drylands"), The Royal Society ("DRIER", grant no. CHL\R1\180485), and the European Union's Horizon 2020 programme ("DOWN2EARTH", grant no. 869550).

Funding

This work was supported by Horizon 2020 Framework Programme, 101209082, 869550; UK Research and Innovation, Strategic Impact Funding; Natural Environment Research Council, NE/T005645/1, NE/P017819/1; Leverhulme Trust, RF-2023-591\4; Royal Society, CHL\R1\180485; National Science Foundation, BCS-1660490, EAR-1700555; U.S. Department of Defense, RC18-1006; International Atomic Energy Agency, CRP D12014.

Data Availability Statement

The DRYPv1.0 code is archived at https://doi.org/10.5281/zenodo.5061988 (Quichimbo et al. 2021) and available at https://github.com/AndresQuichimbo/DRYP (last access: 10 October 2025). Our dataset contains modified Copernicus Climate Change Service information (1981–present) available at https://cds.climate.copernicus.eu/cdsapp#!/dataset/reanalysis-era5-single-levels?tab=form (Copernicus Climate Change Service, Climate Data Store 2018). The streamflow dataset used in this research is publicly available at https://www.tucson.ars.ag.gov/dap/runoff_aggregate.asp (Sourthwest Watershed Research Center, Goodrich (2020)). The soil moisture dataset is publicly available at http://cosmos.hwr.arizona.edu/Probes/StationDat/010/index.php (Atmospheric and Geospace Sciences Division of the National Science Foundation). The flux tower data are publicly available at https://doi.org/10.17190/AMF/1246112 (Scott 2021).

References

Abdulrazzak, M. J. 1995. "Losses of Flood Water From Alluvial Channels." *Arid Soil Research and Rehabilitation* 9: 15–24. https://doi.org/10.1080/15324989509385870.

Albergel, C., E. Dutra, S. Munier, et al. 2018. "ERA-5 and ERA-Interim Driven ISBA Land Surface Model Simulations: Which One Performs Better?" *Hydrology and Earth System Sciences* 22: 3515–3532. https://doi.org/10.5194/hess-22-3515-2018.

Albergel, C., C. Rüdiger, T. Pellarin, et al. 2008. "From Near-Surface to Root-Zone Soil Moisture Using an Exponential Filter: An Assessment of the Method Based on In-Situ Observations and Model Simulations." *Hydrology and Earth System Sciences* 12: 1323–1337. https://doi.org/10.5194/hess-12-1323-2008.

Alfieri, L., V. Lorini, F. A. Hirpa, et al. 2020. "A Global Streamflow Reanalysis for 1980–2018." *Journal of Hydrology X* 6: 100049. https://doi.org/10.1016/j.hydroa.2019.100049.

Allen, G. H., C. H. David, K. M. Andreadis, F. Hossain, and J. S. Famiglietti. 2018. "Global Estimates of River Flow Wave Travel Times and Implications for Low-Latency Satellite Data." *Geophysical Research Letters* 45: 7551–7560. https://doi.org/10.1029/2018GL077914.

Allen, R. G., L. S. Pereira, D. Raes, and M. Smith. 1998. "Crop Evapotranspiration." In *Guidelines for Computing Crop Water Requirements. FAO Irrigation and Drainage Paper 56*. Food and Agriculture Organization of the United Nations (FAO).

Anwar, S. A., A. S. Zakey, S. M. Robaa, and M. M. Abdel Wahab. 2019. "The Influence of Two Land-Surface Hydrology Schemes on the Regional Climate of Africa Using the RegCM4 Model." *Theoretical and Applied Climatology* 136: 1535–1548. https://doi.org/10.1007/s00704-018-2556-8.

Assouline, S., and Y. Mualem. 2002. "Infiltration During Soil Sealing: The Effect of Areal Heterogeneity of Soil Hydraulic Properties." *Water Resources Research* 38: 9. https://doi.org/10.1029/2001WR001168.

Baroni, G., M. Zink, R. Kumar, L. Samaniego, and S. Attinger. 2017. "Effects of Uncertainty in Soil Properties on Simulated Hydrological States and Fluxes at Different Spatio-Temporal Scales." *Hydrology and Earth System Sciences* 21: 2301–2320. https://doi.org/10.5194/hess-21-2301-2017.

Barthel, R., and S. Banzhaf. 2016. "Groundwater and Surface Water Interaction at the Regional-Scale – A Review With Focus on Regional Integrated Models." *Water Resources Management* 30: 1–32. https://doi.org/10.1007/s11269-015-1163-z.

Becker, R., M. Gebremichael, and M. Märker. 2018. "Impact of Soil Surface and Subsurface Properties on Soil Saturated Hydraulic Conductivity in the Semi-Arid Walnut Gulch Experimental Watershed, Arizona, USA." *Geoderma* 322: 112–120. https://doi.org/10.1016/j.geoderma.2018.02.023.

10991085, 2026, 10, Downloaded from https://onlinelibrary.wiley.com/doi/10.1002/hyp.70733 by NICE, National Institute for Health and Care Excellence, Wiley Online Library on [16/10/2026]. See the Terms and Conditions (https://onlinelibrary.wiley.com/terms-and-conditions) on Wiley Online Library for rules of use; OA articles are governed by the applicable Creative Commons License

Beven, K. 1991. "Scale Considerations." In *Recent Advances in the Modeling of Hydrologic Systems, NATO ASI Series*, edited by D. S. Bowles and P. E. O'Connell, 357–371. Springer. https://doi.org/10.1007/978-94-011-3480-4_16.

Beven, K. 1995. "Linking Parameters Across Scales: Subgrid Parameterizations and Scale Dependent Hydrological Models." *Hydrological Processes* 9: 507–525. https://doi.org/10.1002/hyp.3360090504.

Beven, K. 2001. "How Far Can We Go in Distributed Hydrological Modelling?" *Hydrology and Earth System Sciences* 5: 1–12. https://doi.org/10.5194/hess-5-1-2001.

Beven, K. J. 2004. *Rainfall—Runoff Modelling: The Primer*. Wiley.

Beven, K., and A. Binley. 1992. "The Future of Distributed Models: Model Calibration and Uncertainty Prediction." *Hydrological Processes* 6: 279–298.

Bierkens, M. F. P., V. A. Bell, P. Burek, et al. 2015. "Hyper-Resolution Global Hydrological Modelling: What Is Next?" *Hydrological Processes* 29: 310–320. https://doi.org/10.1002/hyp.10391.

Blake, G., K. Michaelides, E. Kendon, M. Cuthbert, and M. Singer. 2025. "The Impact of Convection-Permitting Rainfall on the Dryland Water Balance." *EGUsphere* 1–41: 1154. https://doi.org/10.5194/egusphere-2025-1154.

Blöschl, G. 2001. "Scaling in Hydrology." *Hydrological Processes* 15: 709–711. https://doi.org/10.1002/hyp.432.

Blöschl, G., S. Ardoin-Bardin, M. Bonell, et al. 2007. "At What Scales Do Climate Variability and Land Cover Change Impact on Flooding and Low Flows?" *Hydrological Processes* 21: 1241–1247. https://doi.org/10.1002/hyp.6669.

Blöschl, G., R. B. Grayson, and M. Sivapalan. 1995. "On the Representative Elementary Area (REA) Concept and Its Utility for Distributed Rainfall-Runoff Modelling." *Hydrological Processes* 9: 313–330. https://doi.org/10.1002/hyp.3360090307.

Blöschl, G., and M. Sivapalan. 1995. "Scale Issues in Hydrological Modelling: A Review." *Hydrological Processes* 9: 251–290. https://doi.org/10.1002/hyp.3360090305.

Brooks, R. H., and A. T. Corey. 1964. "Hydraulic Properties of Porous Media, Hydrology Paper No. 3. Colorado State University, Fort Collins."

Chen, S.-A., K. Michaelides, S. W. D. Grieve, and M. B. Singer. 2019. "Aridity Is Expressed in River Topography Globally." *Nature* 573: 573–577. https://doi.org/10.1038/s41586-019-1558-8.

Clapp, R. B., and G. M. Hornberger. 1978. "Empirical Equations for Some Soil Hydraulic Properties." *Water Resources Research* 14: 601–604. https://doi.org/10.1029/WR014i004p00601.

Coes, A. L., and D. R. Pool. 2007. *Ephemeral-Stream Channel and Basin-Floor Infiltration and Recharge in the Sierra Vista Subwatershed of the Upper San Pedro Basin, Southeastern Arizona: Chapter J in Ground-Water Recharge in the Arid and Semiarid Southwestern United States (Professional Paper 1703) (USGS Numbered Series No. 1703-J), Professional Paper*. U.S. Geological Survey.

Copernicus Climate Change Service, Climate Data Store. 2018. ERA5 hourly data on single levels from 1940 to present. Copernicus Climate Change Service (C3S) Climate Data Store (CDS). Accessed December 10, 2026. https://doi.org/10.24381/cds.adbb2d47.

Cortés-Salazar, N., N. Vásquez, N. Mizukami, P. A. Mendoza, and X. Vargas. 2023. "To What Extent Does River Routing Matter in Hydrological Modeling?" *Hydrology and Earth System Sciences* 27: 3505–3524. https://doi.org/10.5194/hess-27-3505-2023.

Costigan, K. H., M. J. Kennard, C. Leigh, E. Sauquet, T. Datry, and A. J. Boulton. 2017. "Chapter 2.2—Flow Regimes in Intermittent Rivers and Ephemeral Streams." In *Intermittent Rivers and Ephemeral Streams*, 51–78. Academic Press. https://doi.org/10.1016/B978-0-12-803835-2.00003-6.

Craig, J. R., G. Liu, and E. D. Soulis. 2010. "Runoff–Infiltration Partitioning Using an Upscaled Green–Ampt Solution." *Hydrological Processes* 24: 2328–2334. https://doi.org/10.1002/hyp.7601.

Crow, W. T., F. Chen, R. H. Reichle, Y. Xia, and Q. Liu. 2018. "Exploiting Soil Moisture, Precipitation, and Streamflow Observations to Evaluate Soil Moisture/Runoff Coupling in Land Surface Models." *Geophysical Research Letters* 45: 4869–4878. https://doi.org/10.1029/2018GL077193.

Cudennec, C., C. Leduc, and D. Koutsoyiannis. 2007. "Dryland Hydrology in Mediterranean Regions—A Review." *Hydrological Sciences Journal* 52: 1077–1087. https://doi.org/10.1623/hysj.52.6.1077.

Cuthbert, M. O. 2014. "Straight Thinking About Groundwater Recession." *Water Resources Research* 50: 2407–2424. https://doi.org/10.1002/2013WR014060.

Cuthbert, M. O., R. I. Acworth, M. S. Andersen, et al. 2016. "Understanding and Quantifying Focused, Indirect Groundwater Recharge From Ephemeral Streams Using Water Table Fluctuations." *Water Resources Research* 52: 827–840. https://doi.org/10.1002/2015WR017503.

Cuthbert, M. O., T. Gleeson, N. Moosdorf, et al. 2019. "Global Patterns and Dynamics of Climate–Groundwater Interactions." *Nature Climate Change* 9: 137–141. https://doi.org/10.1038/s41558-018-0386-4.

Dai, Y., W. Shangguan, N. Wei, et al. 2019. "A Review of the Global Soil Property Maps for Earth System Models." *Soil* 5: 137–158. https://doi.org/10.5194/soil-5-137-2019.

Dai, Y., Q. Xin, N. Wei, et al. 2019. "A Global High-Resolution Data Set of Soil Hydraulic and Thermal Properties for Land Surface Modeling." *Journal of Advances in Modeling Earth Systems* 11: 2996–3023. https://doi.org/10.1029/2019MS001784.

de Graaf, I. E. M., E. H. Sutanudjaja, L. P. H. van Beek, and M. F. P. Bierkens. 2015. "A High-Resolution Global-Scale Groundwater Model." *Hydrology and Earth System Sciences* 19: 823–837. https://doi.org/10.5194/hess-19-823-2015.

Desilets, D., M. Zreda, and T. P. A. Ferré. 2010. "Nature's Neutron Probe: Land Surface Hydrology at an Elusive Scale With Cosmic Rays." *Water Resources Research* 46: W11505. https://doi.org/10.1029/2009WR008726.

Dimitrova-Petrova, K., J. Geris, E. Mark Wilkinson, et al. 2020. "Opportunities and Challenges in Using Catchment-Scale Storage Estimates From Cosmic Ray Neutron Sensors for Rainfall-Runoff Modelling." *Journal of Hydrology* 586: 124878. https://doi.org/10.1016/j.jhydrol.2020.124878.

Dunkerley, D. 2018. "How Is Overland Flow Produced Under Intermittent Rain? An Analysis Using Plot-Scale Rainfall Simulation on Dryland Soils." *Journal of Hydrology* 556: 119–130. https://doi.org/10.1016/j.jhydrol.2017.11.003.

Emmerich, W. E., and C. L. Verdugo. 2008. "Long-Term Carbon Dioxide and Water Flux Database, Walnut Gulch Experimental Watershed, Arizona, United States." *Water Resources Research* 44: W05S09. https://doi.org/10.1029/2006WR005693.

Faurès, J.-M., D. C. Goodrich, D. A. Woolhiser, and S. Sorooshian. 1995. "Impact of Small-Scale Spatial Rainfall Variability on Runoff Modeling." *Journal of Hydrology* 173: 309–326. https://doi.org/10.1016/0022-1694(95)02704-S.

Fenicia, F., H. H. G. Savenije, P. Matgen, and L. Pfister. 2008. "Understanding Catchment Behavior Through Stepwise Model Concept Improvement." *Water Resources Research* 44: WR005563. https://doi.org/10.1029/2006WR005563.

Franz, T. E., M. Zreda, T. P. A. Ferre, et al. 2012. "Measurement Depth of the Cosmic Ray Soil Moisture Probe Affected by Hydrogen From

10991085, 2026, 10, Downloaded from https://onlinelibrary.wiley.com/doi/10.1002/hyp.70733 by NICE, National Institute for Health and Care Excellence, Wiley Online Library on [16/10/2026]. See the Terms and Conditions (https://onlinelibrary.wiley.com/terms-and-conditions) on Wiley Online Library for rules of use; OA articles are governed by the applicable Creative Commons License

Various Sources." *Water Resources Research* 48: W08515. https://doi.org/10.1029/2012WR011871.

Franz, T. E., M. Zreda, R. Rosolem, and T. P. A. Ferre. 2013. "A Universal Calibration Function for Determination of Soil Moisture With Cosmic-Ray Neutrons." *Hydrology and Earth System Sciences* 17: 453–460. https://doi.org/10.5194/hess-17-453-2013.

García, M., I. Sandholt, P. Ceccato, et al. 2013. "Actual Evapotranspiration in Drylands Derived From In-Situ and Satellite Data: Assessing Biophysical Constraints." *Remote Sensing of Environment* 131: 103–118. https://doi.org/10.1016/j.rse.2012.12.016.

Glenn, E. P., R. L. Scott, U. Nguyen, and P. L. Nagler. 2015. "Wide-Area Ratios of Evapotranspiration to Precipitation in Monsoon-Dependent Semiarid Vegetation Communities." *Journal of Arid Environments* 117: 84–95. https://doi.org/10.1016/j.jaridenv.2015.02.010.

Goodrich, D. 2020. Walnut Gulch Experimental Watershed, Arizona (Runoff). USDA Agricultural Research Service Dataset. https://hdl.handle.net/10113/AA25763.

Goodrich, D., I. Burns, C. Unkrich, et al. 2012. "KINEROS2/AGWA: Model Use, Calibration, and Validation." *Transactions of the ASABE* 55, no. 4: 1561–1574. https://doi.org/10.13031/2013.42264.

Goodrich, D. C., J.-M. Faurès, D. A. Woolhiser, L. J. Lane, and S. Sorooshian. 1995. "Measurement and Analysis of Small-Scale Convective Storm Rainfall Variability." *Journal of Hydrology* 173: 283–308. https://doi.org/10.1016/0022-1694(95)02703-R.

Goodrich, D. C., T. O. Keefer, C. L. Unkrich, et al. 2008. "Long-Term Precipitation Database, Walnut Gulch Experimental Watershed, Arizona, United States." *Water Resources Research* 44: W05S04. https://doi.org/10.1029/2006WR005782.

Goodrich, D. C., W. G. Kepner, L. R. Levick, and P. J. Wigington. 2018. "Southwestern Intermittent and Ephemeral Stream Connectivity." *JAWRA Journal of the American Water Resources Association* 54: 400–422. https://doi.org/10.1111/1752-1688.12636.

Goodrich, D. C., L. J. Lane, R. M. Shillito, S. N. Miller, K. H. Syed, and D. A. Woolhiser. 1997. "Linearity of Basin Response as a Function of Scale in a Semiarid Watershed." *Water Resources Research* 33: 2951–2965. https://doi.org/10.1029/97WR01422.

Goodrich, D. C., T. J. Schmugge, T. J. Jackson, et al. 1994. "Runoff Simulation Sensitivity to Remotely Sensed Initial Soil Water Content." *Water Resources Research* 30: 1393–1405. https://doi.org/10.1029/93WR03083.

Goodrich, D. C., D. G. Williams, C. L. Unkrich, et al. 2013. *Comparison of Methods to Estimate Ephemeral Channel Recharge, Walnut Gulch, San Pedro River Basin, Arizona, in: Groundwater Recharge in a Desert Environment: The Southwestern United States*, 77–99. American Geophysical Union (AGU).

Green, T. R., M. Taniguchi, H. Kooi, et al. 2011. "Beneath the Surface of Global Change: Impacts of Climate Change on Groundwater." *Journal of Hydrology* 405: 532–560. https://doi.org/10.1016/j.jhydrol.2011.05.002.

Green, W. H., and G. A. Ampt. 1911. "Studies on Soil Phyics. 1, the Flow of Air and Water Through Soils." *Journal of Agricultural Science* 4: 1–24. https://doi.org/10.1017/S0021859600001441.

Grogan, D. S., S. Zuidema, A. Prusevich, W. M. Wollheim, S. Glidden, and R. B. Lammers. 2022. "Water Balance Model (WBM) v.1.0.0: A Scalable Gridded Global Hydrologic Model With Water-Tracking Functionality." *Geoscientific Model Development* 15: 7287–7323. https://doi.org/10.5194/gmd-15-7287-2022.

Heilman, P., M. H. Nichols, D. C. Goodrich, S. N. Miller, and D. P. Guertin. 2008. "Geographic Information Systems Database, Walnut Gulch Experimental Watershed, Arizona, United States." *Water Resources Research* 44: W05S11. https://doi.org/10.1029/2006WR005777.

Hersbach, H., B. Bell, P. Berrisford, et al. 2020. "The ERA5 Global Reanalysis." *Quarterly Journal of the Royal Meteorological Society* 146, no. 730: 1999–2049. https://doi.org/10.1002/qj.3803.

Hooke, J. M. 2019. "Extreme Sediment Fluxes in a Dryland Flash Flood." *Scientific Reports* 9: 1686. https://doi.org/10.1038/s41598-019-38537-3.

Huang, J., Y. Li, C. Fu, et al. 2017. "Dryland Climate Change: Recent Progress and Challenges." *Reviews of Geophysics* 55: 719–778. https://doi.org/10.1002/2016RG000550.

Huang, J., H. Yu, X. Guan, G. Wang, and R. Guo. 2015. "Accelerated Dryland Expansion Under Climate Change." *Nature Climate Change* 6: 2837. https://doi.org/10.1038/nclimate2837.

Huang, Y., A. Bárdossy, and K. Zhang. 2019. "Sensitivity of Hydrological Models to Temporal and Spatial Resolutions of Rainfall Data." *Hydrology and Earth System Sciences* 23: 2647–2663. https://doi.org/10.5194/hess-23-2647-2019.

IPCC6. 2021. *Climate Change 2021: The Physical Science Basis. Contribution of Working Group I to the Sixth Assessment Report of the Intergovernmental Panel on Climate Change*. Cambridge University Press.

Jaeger, K. L., N. A. Sutfin, S. Tooth, K. Michaelides, and M. Singer. 2017. "Chapter 2.1—Geomorphology and Sediment Regimes of Intermittent Rivers and Ephemeral Streams." In *Intermittent Rivers and Ephemeral Streams*, edited by T. Datry, N. Bonada, and A. Boulton, 21–49. Academic Press. https://doi.org/10.1016/B978-0-12-803835-2.00002-4.

Kebede, S., K. Charles, S. Godfrey, A. MacDonald, and R. G. Taylor. 2021. "Regional-Scale Interactions Between Groundwater and Surface Water Under Changing Aridity: Evidence From the River Awash Basin, Ethiopia." *Hydrological Sciences Journal* 66: 450–463. https://doi.org/10.1080/02626667.2021.1874613.

Keefer, T. O., M. S. Moran, and G. B. Paige. 2008. "Long-Term Meteorological and Soil Hydrology Database, Walnut Gulch Experimental Watershed, Arizona, United States." *Water Resources Research* 44: W05S07. https://doi.org/10.1029/2006WR005702.

Keppel, R. V., and K. G. Renard. 1962. "Transmission Losses in Ephemeral Stream Beds." *Journal of the Hydraulics Division* 88: 59–68.

Kibler, C. L., A. T. Trugman, D. A. Roberts, et al. 2023. "Evapotranspiration Regulates Leaf Temperature and Respiration in Dryland Vegetation." *Agricultural and Forest Meteorology* 339: 109560. https://doi.org/10.1016/j.agrformet.2023.109560.

Kipkemoi, I., K. Michaelides, R. Rosolem, and M. B. Singer. 2021. "Climatic Expression of Rainfall on Soil Moisture Dynamics in Drylands." *Hydrology and Earth System Sciences Discussions* 1–24: 48. https://doi.org/10.5194/hess-2021-48.

Krause, P., D. P. Boyle, and F. Bäse. 2005. "Comparison of Different Efficiency Criteria for Hydrological Model Assessment." *Advances in Geosciences* 5: 89–97.

Lahmers, T. M., H. Gupta, C. L. Castro, et al. 2019. "Enhancing the Structure of the WRF-Hydro Hydrologic Model for Semiarid Environments." *Journal of Hydrometeorology* 20: 691–714. https://doi.org/10.1175/JHM-D-18-0064.1.

Larned, S. T., T. Datry, D. B. Arscott, and K. Tockner. 2010. "Emerging Concepts in Temporary-River Ecology." *Freshwater Biology* 55: 717–738. https://doi.org/10.1111/j.1365-2427.2009.02322.x.

Laronne, J. B., and L. Reid. 1993. "Very High Rates of Bedload Sediment Transport by Ephemeral Desert Rivers." *Nature* 366: 148–150. https://doi.org/10.1038/366148a0.

Leigh, C., and T. Datry. 2017. "Drying as a Primary Hydrological Determinant of Biodiversity in River Systems: A Broad-Scale Analysis." *Ecography* 40: 487–499. https://doi.org/10.1111/ecog.02230.

10991085, 2026, 10, Downloaded from https://onlinelibrary.wiley.com/doi/10.1002/hyp.70733 by NICE, National Institute for Health and Care Excellence, Wiley Online Library on [16/10/2026]. See the Terms and Conditions (https://onlinelibrary.wiley.com/terms-and-conditions) on Wiley Online Library for rules of use; OA articles are governed by the applicable Creative Commons License

Lesschen, J. P., J. J. Stoorvogel, and E. M. A. Smaling. 2004. "Scaling Soil Nutrient Balances." In *Enabling Mesolevel Applications for African Realities*. Food and Agriculture Organization of the United Nations.

Liu, J., B. A. Engel, Y. Wang, Y. Wu, Z. Zhang, and M. Zhang. 2019. "Runoff Response to Soil Moisture and Micro-Topographic Structure on the Plot Scale." *Scientific Reports* 9: 2532. https://doi.org/10.1038/s41598-019-39409-6.

Lopes, V. L. 1996. "On the Effect of Uncertainty in Spatial Distribution of Rainfall on Catchment Modelling." *Catena* 28: 107–119. https://doi.org/10.1016/S0341-8162(96)00030-6.

Mayes, M., K. K. Caylor, M. B. Singer, J. C. Stella, D. Roberts, and P. Nagler. 2020. "Climate Sensitivity of Water Use by Riparian Woodlands at Landscape Scales." *Hydrological Processes* 34: 4884–4903. https://doi.org/10.1002/hyp.13942.

Merz, B., and E. J. Plate. 1997. "An Analysis of the Effects of Spatial Variability of Soil and Soil Moisture on Runoff." *Water Resources Research* 33: 2909–2922. https://doi.org/10.1029/97WR02204.

Merz, R., J. Parajka, and G. Blöschl. 2009. "Scale Effects in Conceptual Hydrological Modeling." *Water Resources Research* 45: WR007872. https://doi.org/10.1029/2009WR007872.

Michaelides, K., R. Hollings, M. B. Singer, M. H. Nichols, and M. A. Nearing. 2018. "Spatial and Temporal Analysis of Hillslope–Channel Coupling and Implications for the Longitudinal Profile in a Dryland Basin." *Earth Surface Processes and Landforms* 43: 1608–1621. https://doi.org/10.1002/esp.4340.

Michaelides, K., and M. B. Singer. 2014. "Impact of Coarse Sediment Supply From Hillslopes to the Channel in Runoff-Dominated, Dryland Fluvial Systems." *Journal of Geophysical Research - Earth Surface* 119: 1205–1221. https://doi.org/10.1002/2013JF002959.

Michaelides, K., and M. D. Wilson. 2007. "Uncertainty in Predicted Runoff due to Patterns of Spatially Variable Infiltration." *Water Resources Research* 43: W02415. https://doi.org/10.1029/2006WR005039.

Miller, S. N., A. Youberg, D. P. Guertin, and D. C. Goodrich. 2000. "Channel Morphology Investigations Using Geographic Information Systems and Field Research." In *Land Stewardship in the 21st Century: The Contributions of Watershed Management, 13–16 March 2000*, 415–419. US Department of Agriculture, Forest Service, Rocky Mountain Research Station.

Montzka, C., M. Herbst, L. Weihermüller, A. Verhoef, and H. Vereecken. 2017. "A Global Data Set of Soil Hydraulic Properties and Sub-Grid Variability of Soil Water Retention and Hydraulic Conductivity Curves." *Earth System Science Data* 9: 529–543. https://doi.org/10.5194/essd-9-529-2017.

Nash, I. E., and I. V. Sutcliffe. 1970. "River Flow Forecasting Through Conceptual Models." *Journal of Hydrology* 10: 282–290.

Ó Dochartaigh, B. E., A. M. MacDonald, W. G. Darling, A. G. Hughes, J. X. Li, and L. A. Shi. 2010. "Determining Groundwater Degradation From Irrigation in Desert-Marginal Northern China." *Hydrogeology Journal* 18: 1939–1952. https://doi.org/10.1007/s10040-010-0644-7.

Osborn, H. B., and L. Lane. 1969. "Precipitation-Runoff Relations for Very Small Semiarid Rangeland Watersheds." *Water Resources Research* 5: 419–425. https://doi.org/10.1029/WR005i002p00419.

Osterkamp, W. R. 2008. "Geology, Soils, and Geomorphology of the Walnut Gulch Experimental Watershed, Tombstone, Arizona." *Journal of the Arizona-Nevada Academy of Science* 40: 136–154. https://doi.org/10.2181/1533-6085-40.2.136.

Park, S. W., L. Linsen, O. Kreylos, J. D. Owens, and B. Hamann. 2006. "Discrete Sibson Interpolation." *IEEE Transactions on Visualization and Computer Graphics* 12: 243–253. https://doi.org/10.1109/TVCG.2006.27.

Pelletier, J. D., P. D. Broxton, P. Hazenberg, et al. 2016. "A Gridded Global Data Set of Soil, Intact Regolith, and Sedimentary Deposit Thicknesses for Regional and Global Land Surface Modeling." *Journal of Advances in Modeling Earth Systems* 8: 41–65. https://doi.org/10.1002/2015MS000526.

Philip, J. R. 1957. "Theory of Infiltration: The Infiltration Equation and Its Solutions." *Soil Science* 171: S34–S46.

Philip, J. R. 1987. "The Infiltration Joining Problem." *Water Resources Research* 23: 2239–2245. https://doi.org/10.1029/WR023i012p02239.

Pilgrim, D. H., T. G. Chapman, and D. G. Doran. 1988. "Problems of Rainfall-Runoff Modelling in Arid and Semiarid Regions." *Hydrological Sciences Journal* 33: 379–400. https://doi.org/10.1080/02626668809491261.

Pool, D. R., and W. Schmidt. 1997. *Measurement of Ground-Water Storage Change and Specific Yield Using the Temporal-Gravity Method Near Rillito Creek*. U.S. Department of the Interior, U.S. Geological Survey.

Power, D., M. A. Rico-Ramirez, S. Desilets, D. Desilets, and R. Rosolem. 2021. *Cosmic-Ray Neutron Sensor PYthon Tool (Crspy): An Open-Source Tool for the Processing of Cosmic-Ray Neutron and Soil Moisture Data*. Geosci.

Qiu, Y., J. S. Famiglietti, A. Behrangi, et al. 2025. "The Strong Impact of Precipitation Intensity on Groundwater Recharge and Terrestrial Water Storage Change in Arizona, a Typical Dryland." *Geophysical Research Letters* 52: e2025GL114747. https://doi.org/10.1029/2025GL114747.

Quichimbo, E. A., M. B. Singer, and M. O. Cuthbert. 2020. "Characterising Groundwater–Surface Water Interactions in Idealised Ephemeral Stream Systems." *Hydrological Processes* 34: 3792–3806. https://doi.org/10.1002/hyp.13847.

Quichimbo, E. A., M. B. Singer, K. Michaelides, D. E. J. Hobley, R. Rosolem, and M. O. Cuthbert. 2021. "DRYP 1.0: A Parsimonious Hydrological Model of DRYland Partitioning of the Water Balance." *Geoscientific Model Development* 14: 6893–6917. https://doi.org/10.5194/gmd-14-6893-2021.

Quichimbo, E. A., M. B. Singer, K. Michaelides, et al. 2023. "Assessing the Sensitivity of Modelled Water Partitioning to Global Precipitation Datasets in a Data-Scarce Dryland Region." *Hydrological Processes* 37: e15047. https://doi.org/10.1002/hyp.15047.

Rawls, W. J., D. L. Brakensiek, and K. E. Saxtonn. 1982. "Estimation of Soil Water Properties." *Translator* 25: 1316–1320. https://doi.org/10.13031/2013.33720.

Renard, K. G. 1970. *The Hydrology of Semiarid Rangeland Watersheds*. Agricultural Research Service, United States Department of Agriculture.

Renard, K. G., M. H. Nichols, D. A. Woolhiser, and H. B. Osborn. 2008. "A Brief Background on the U.S. Department of Agriculture Agricultural Research Service Walnut Gulch Experimental Watershed." *Water Resources Research* 44: W05S02. https://doi.org/10.1029/2006WR005691.

Reynolds, J. F., D. M. S. Smith, E. F. Lambin, et al. 2007. "Global Desertification: Building a Science for Dryland Development." *Science* 316: 847–851. https://doi.org/10.1126/science.1131634.

Richardson, A. D., D. Y. Hollinger, G. G. Burba, et al. 2006. "A Multi-Site Analysis of Random Error in Tower-Based Measurements of Carbon and Energy Fluxes." *Agricultural and Forest Meteorology* 136: 1–18. https://doi.org/10.1016/j.agrformet.2006.01.007.

Rosolem, R., W. J. Shuttleworth, M. Zreda, T. E. Franz, X. Zeng, and S. A. Kurc. 2013. "The Effect of Atmospheric Water Vapor on Neutron Count in the Cosmic-Ray Soil Moisture Observing System." *Journal of Hydrometeorology* 14: 1659–1671. https://doi.org/10.1175/JHM-D-12-0120.1.

Sabathier, R., M. B. Singer, J. C. Stella, D. A. Roberts, and K. K. Caylor. 2021. "Vegetation Responses to Climatic and Geologic Controls on Water Availability in Southeastern Arizona." *Environmental Research Letters* 16: 064029. https://doi.org/10.1088/1748-9326/abfe8c.

10991085, 2026, 10, Downloaded from https://onlinelibrary.wiley.com/doi/10.1002/hyp.70733 by NICE, National Institute for Health and Care Excellence, Wiley Online Library on [16/10/2026]. See the Terms and Conditions (https://onlinelibrary.wiley.com/terms-and-conditions) on Wiley Online Library for rules of use; OA articles are governed by the applicable Creative Commons License

Scanlon, B. R., K. E. Keese, A. L. Flint, et al. 2006. "Global Synthesis of Groundwater Recharge in Semiarid and Arid Regions." *Hydrological Processes* 20: 3335–3370. https://doi.org/10.1002/hyp.6335.

Schaake, J. C., V. I. Koren, Q.-Y. Duan, K. Mitchell, and F. Chen. 1996. "Simple Water Balance Model for Estimating Runoff at Different Spatial and Temporal Scales." *Journal of Geophysical Research-Atmospheres* 101: 7461–7475. https://doi.org/10.1029/95JD02892.

Scheidegger, J. M., C. R. Jackson, S. Muddu, S. K. Tomer, and R. Filgueira. 2021. "Integration of 2D Lateral Groundwater Flow Into the Variable Infiltration Capacity (VIC) Model and Effects on Simulated Fluxes for Different Grid Resolutions and Aquifer Diffusivities." *Water* 13: 663. https://doi.org/10.3390/w13050663.

Schmidt, A., C. Hanson, W. S. Chan, and B. E. Law. 2012. "Empirical Assessment of Uncertainties of Meteorological Parameters and Turbulent Fluxes in the AmeriFlux Network." *Journal of Geophysical Research: Biogeosciences* 117: G04014. https://doi.org/10.1029/2012JG002100.

Schreiner-McGraw, A., H. Ajami, and E. R. Vivoni. 2019. "Extreme Weather Events and Transmission Losses in Arid Streams." *Environmental Research Letters* 14: 084002. https://doi.org/10.1088/1748-9326/ab2949.

Schreiner-McGraw, A. P., and E. R. Vivoni. 2018. "On the Sensitivity of Hillslope Runoff and Channel Transmission Losses in Arid Piedmont Slopes." *Water Resources Research* 54: 4498–4518. https://doi.org/10.1029/2018WR022842.

Scott, R. L. 2010. "Using Watershed Water Balance to Evaluate the Accuracy of Eddy Covariance Evaporation Measurements for Three Semiarid Ecosystems." *Agricultural and Forest Meteorology* 150: 219–225. https://doi.org/10.1016/j.agrformet.2009.11.002.

Scott, R. 2021. AmeriFlux BASE US-Wkg Walnut Gulch Kendall Grasslands, Ver. 28-5, AmeriFlux AMP, (Dataset). https://doi.org/10.17190/AMF/1246112.

Scott, R. L., J. A. Biederman, E. P. Hamerlynck, and G. A. Barron-Gafford. 2015. "The Carbon Balance Pivot Point of Southwestern U.S. Semiarid Ecosystems: Insights From the 21st Century Drought." *Journal of Geophysical Research: Biogeosciences* 120: 2612–2624. https://doi.org/10.1002/2015JG003181.

Seddon, D., J. J. Kashaigili, R. G. Taylor, M. O. Cuthbert, C. Mwihumbo, and A. M. MacDonald. 2021. "Focused Groundwater Recharge in a Tropical Dryland: Empirical Evidence From Central, Semi-Arid Tanzania." *Journal of Hydrology: Regional Studies* 37: 100919. https://doi.org/10.1016/j.ejrh.2021.100919.

Shanafield, M., and P. G. Cook. 2014. "Transmission Losses, Infiltration and Groundwater Recharge Through Ephemeral and Intermittent Streambeds: A Review of Applied Methods." *Journal of Hydrology* 511: 518–529. https://doi.org/10.1016/j.jhydrol.2014.01.068.

Singer, M. B., D. T. Asfaw, R. Rosolem, et al. 2021. "Hourly Potential Evapotranspiration at 0.1° Resolution for the Global Land Surface From 1981-Present." *Scientific Data* 8: 224. https://doi.org/10.1038/s41597-021-01003-9.

Singer, M. B., and K. Michaelides. 2014. "How Is Topographic Simplicity Maintained in Ephemeral Dryland Channels?" *Geology* 42: 1091–1094. https://doi.org/10.1130/G36267.1.

Singer, M. B., and K. Michaelides. 2017. "Deciphering the Expression of Climate Change Within the Lower Colorado River Basin by Stochastic Simulation of Convective Rainfall." *Environmental Research Letters* 12: 104011. https://doi.org/10.1088/1748-9326/aa8e50.

Skirvin, S., M. Kidwell, S. Biedenbender, et al. 2008. "Vegetation Data, Walnut Gulch Experimental Watershed, Arizona, United States." *Water Resources Research* 44: WR005724. https://doi.org/10.1029/2006WR005724.

Smith, R. E., D. L. Chery, K. G. Renard, and W. R. Gwinn. 1982. *Supercritical Flow Flumes for Measuring Sediment-Laden Flow (Technical Report No. 1655)*. USDA ARS. U.S. Dep. of Agriculture.

Stephens, D. B. 1994. "A Perspective on Diffuse Natural Recharge Mechanisms in Areas of Low Precipitation." *Soil Science Society of America Journal* 58: 40–48. https://doi.org/10.2136/sssaj1994.03615995005800010006x.

Steward, A. L., D. von Schiller, K. Tockner, J. C. Marshall, and S. E. Bunn. 2012. "When the River Runs Dry: Human and Ecological Values of Dry Riverbeds." *Frontiers in Ecology and the Environment* 10: 202–209. https://doi.org/10.1890/110136.

Stewart, R. D., A. S. Bhaskar, A. J. Parolari, et al. 2019. "An Analytical Approach to Ascertain Saturation-Excess Versus Infiltration-Excess Overland Flow in Urban and Reference Landscapes." *Hydrological Processes* 33: 3349–3363. https://doi.org/10.1002/hyp.13562.

Stone, J. J., M. H. Nichols, D. C. Goodrich, and J. Buono. 2008. "Long-Term Runoff Database, Walnut Gulch Experimental Watershed, Arizona, United States." *Water Resources Research* 44: W05S05. https://doi.org/10.1029/2006WR005733.

Tarek, M., F. P. Brissette, and R. Arsenault. 2020. "Evaluation of the ERA5 Reanalysis as a Potential Reference Dataset for Hydrological Modelling Over North America." *Hydrology and Earth System Sciences* 24: 2527–2544. https://doi.org/10.5194/hess-24-2527-2020.

Taylor, R. G., M. C. Todd, L. Kongola, et al. 2013. "Evidence of the Dependence of Groundwater Resources on Extreme Rainfall in East Africa." *Nature Climate Change* 3: 374–378. https://doi.org/10.1038/nclimate1731.

Twine, T. E., W. P. Kustas, J. M. Norman, et al. 2000. "Correcting Eddy-Covariance Flux Underestimates Over a Grassland." *Agricultural and Forest Meteorology* 103: 279–300. https://doi.org/10.1016/S0168-1923(00)00123-4.

USBR. 1977. *Central Arizona Project, Geology and Ground-Water Resources Report, Maricopa and Pinal Counties, Arizona, October 1977*. Bureau of Reclamation.

Vereecken, H., L. Weihermüller, S. Assouline, et al. 2019. "Infiltration From the Pedon to Global Grid Scales: An Overview and Outlook for Land Surface Modeling." *Vadose Zone Journal* 18: 180191. https://doi.org/10.2136/vzj2018.10.0191.

Wagner, W., G. Lemoine, and H. Rott. 1999. "A Method for Estimating Soil Moisture From ERS Scatterometer and Soil Data." *Remote Sensing of Environment* 70: 191–207. https://doi.org/10.1016/S0034-4257(99)00036-X.

Walker, W. R. 1989. "Guidelines for Designing and Evaluating Surface Irrigation Systems." In *FAO Irrigation and Drainage Paper 45*. FAO.

Wallace, D. E., and K. G. Renard. 1967. "Contribution to Regional Water Table From Transmission Losses of Ephemeral Streambeds." *Transactions of ASAE* 10: 786–789. https://doi.org/10.13031/2013.39786.

Wang, L., W. Chen, G. Huang, and G. Zeng. 2017. "Changes of the Transitional Climate Zone in East Asia: Past and Future." *Climate Dynamics* 49: 1463–1477. https://doi.org/10.1007/s00382-016-3400-4.

Warter, M. M., M. B. Singer, M. O. Cuthbert, et al. 2020. "Onset and Propagation of Drought Into Soil Moisture and Vegetation Responses During the 2012–2019 Drought in Southern California." *Hydrology and Earth System Sciences Discussions* 1–35: 479. https://doi.org/10.5194/hess-2020-479.

Wen, H., S. L. Brantley, K. J. Davis, J. M. Duncan, and L. Li. 2021. "The Limits of Homogenization: What Hydrological Dynamics Can a Simple Model Represent at the Catchment Scale? Water Resour." *Resource* 57: e2020WR029528. https://doi.org/10.1029/2020WR029528.

10991085, 2026, 10, Downloaded from https://onlinelibrary.wiley.com/doi/10.1002/hyp.70733 by NICE, National Institute for Health and Care Excellence, Wiley Online Library on [16/10/2026]. See the Terms and Conditions (https://onlinelibrary.wiley.com/terms-and-conditions) on Wiley Online Library for rules of use; OA articles are governed by the applicable Creative Commons License

Wheater, H., S. Sorooshian, and K. D. Sharma, eds. 2007. *Hydrological Modelling in Arid and Semi-Arid Areas*. 1st ed. Cambridge University Press.

Wilcox, B. P., Y. Huang, and J. W. Walker. 2008. "Long-Term Trends in Streamflow From Semiarid Rangelands: Uncovering Drivers of Change." *Global Change Biology* 14: 1676–1689. https://doi.org/10.1111/j.1365-2486.2008.01578.x.

Wood, E. F., J. K. Roundy, T. J. Troy, et al. 2011. "Hyperresolution Global Land Surface Modeling: Meeting a Grand Challenge for Monitoring Earth's Terrestrial Water." *Water Resources Research* 47: WR010090. https://doi.org/10.1029/2010WR010090.

Woolhiser, D. A. 1989. *KINEROS, A Kinematic Runoff and Erosion Model*. Use Man.

Yair, A., and H. Lavee. 1982. "Factors Affecting the Spatial Variability of Runoff Generation Over Arid Hillslopes, Southern Israel." *Israel Journal of Earth Sciences* 31: 133–143.

Yatheendradas, S., T. Wagener, H. Gupta, et al. 2008. "Understanding Uncertainty in Distributed Flash Flood Forecasting for Semiarid Regions." *Water Resources Research* 44: WR005940. https://doi.org/10.1029/2007WR005940.

Zoccatelli, D., F. Marra, M. Armon, Y. Rinat, J. A. Smith, and E. Morin. 2019. "Contrasting Rainfall-Runoff Characteristics of Floods in Desert and Mediterranean Basins." *Hydrology and Earth System Sciences* 23: 2665–2678. https://doi.org/10.5194/hess-23-2665-2019.

Zreda, M., W. J. Shuttleworth, X. Zeng, et al. 2012. "COSMOS: The COsmic-Ray Soil Moisture Observing System." *Hydrology and Earth System Sciences* 16: 4079–4099. https://doi.org/10.5194/hess-16-4079-2012.

Supporting Information

Additional supporting information can be found online in the Supporting Information section. **Table S1:** Soil hydraulic parameters for general textural classes, based on Rawls et al. (1982) and Clapp and Hornberger (1978): n is the porosity, b is the pore size distribution parameter, and ψ is the maximum soil matric potential. **Table S2:** Prior parameter range for each component and infiltration approach considered in the Monte Carlo analysis; parameters starting with 'k' mean that it is a factor of the model parameter. Infiltration approaches are specified as P for Philip's model, G for Upscaled Green and Ampt, S for Schaake model, and M for Modified Green and Ampt. **Figure S1:** Indices estimated for the best models selected according to the likelihood measure 'p' based on the evaluation of only flume F01, and soil moisture and AET at Kendall. (a) Estimated 'p' against the number of valid models resulted from the Monte Carlo analysis for different grid size, time-step, and infiltration approach. (b) NSE for the soil moisture estimated at the Kendall location against NSE of the evapotranspiration at Kendall location. (c) R^2 of flumes F06 against F01. Part d, e and (f) represent the NSE against the PBIAS for the three flumes located along the main channel, flume F01, F02 and F06, flumes F02 and F06 were added only for comparison. Results at 5-km grid size were evaluated only at flume F01. Models are labelled as P = Philips, S = Schaake, G = upscaled Green and Ampt, and M = modified Green and Ampt. Models at 5-km grid size do not consider the evapotranspiration in the evaluation. **Figure S2:** Distribution of parameter factors (a) kK_{sat}, (b) kD_{root}, (c) kK_{ch}, and (d) kT for behavioural simulations based on evaluation at flume F01, and soil moisture and AET at Kendall. Models using different infiltration methods are represented as P = Philip's, S = Schaake, G = upscaled Green and Ampt, and M = modified Green and Ampt. Models at 5-km grid size are not considered in the evaluation the evapotranspiration. **Figure S3:** Flux distribution as a percentage of rainfall for behavioural model simulations based on the evaluation at flume F01, and soil moisture and AET at Kendall.

10991085, 2026, 10, Downloaded from https://onlinelibrary.wiley.com/doi/10.1002/hyp.70733 by NICE, National Institute for Health and Care Excellence, Wiley Online Library on [16/10/2026]. See the Terms and Conditions (https://onlinelibrary.wiley.com/terms-and-conditions) on Wiley Online Library for rules of use; OA articles are governed by the applicable Creative Commons License

Appendix A: Differences Between Infiltration Approaches

A detailed description of each infiltration approach is provided by Quichimbo et al. (2021). Here, the differences in infiltration dynamics among the four approaches—Schaake (S), Philip (P), Upscaled Green–Ampt (M), and Green–Ampt (G)—are illustrated through a controlled numerical experiment. The simulation was conducted using a constant precipitation intensity of $i = 30\ \text{mm h}^{-1}$ throughout the entire simulation period.

Soil hydraulic properties correspond to a sandy loam soil texture with saturated water content $\theta_{sat} = 0.453\ \text{m}^3\ \text{m}^{-3}$, air-entry pressure at saturation $\psi = 211.01\ \text{mm}$, and pore-size distribution index $\lambda = 4.9$ following Clapp and Hornberger (1978). The saturated hydraulic conductivity was specified as $K_{sat} = 1.6\ \text{cm h}^{-1}$, based on experimental values reported by Craig et al. (2010), with a logarithmic standard deviation of 0.5. The selected precipitation and hydraulic conductivity values correspond to a precipitation-to-conductivity ratio of approximately 0.5, consistent with the experimental configuration of Craig et al. (2010).

Infiltrated water was assumed to drain freely below the soil profile under gravitational conditions. Soil depth was fixed at 200 mm, and the initial soil water content was prescribed at wilting point conditions, $\theta_{wp} = 0.19\ \text{m}^3\ \text{m}^{-3}$. The simulation time step was set to 1 min. All simulations were performed using the infiltration component of DRYP 1.0.

Figure A1a presents the temporal evolution of infiltration rates simulated by the four approaches. For the same values of K_{sat}, precipitation intensity, and initial soil moisture conditions, the M, G, and P approaches exhibit similar initial infiltration rates, as expected from their physical formulations (Quichimbo et al. 2021). However, their temporal evolution differs substantially. The Philip approach (P) maintains the highest infiltration rates for the longest duration (approximately 145 min), whereas the Green–Ampt approach (G) exhibits a rapid decline after approximately 25 min. In contrast, the Upscaled Green–Ampt approach (M) shows a gradual decrease, starting at $t = 25$ min, that eventually exceed the infiltration rates simulated by the Philip approach at time $t = 210$ min. The Schaake approach (S) evolves differently from the other three methods, with infiltration rates decreasing gradually during the first 100 min, followed by a more abrupt decline from approximately 25 to 5 mm h^{-1}.

Figure A1b shows the cumulative infiltration simulated by each model. The P and M approaches produce the largest cumulative infiltration volumes, consistent with the higher infiltration rates shown in Figure A1a. The G approach exhibits a slower but steady increase in cumulative infiltration, whereas the S approach reaches a threshold corresponding to conditions close to saturation of the entire soil layer.

Overall, Figure A1 highlights the substantial differences in infiltration behaviour among the four approaches, despite the use of equivalent hydraulic parameters and boundary conditions. These differences suggest that model calibration may require compensatory adjustments of hydraulic parameters to reproduce comparable infiltration rates and cumulative infiltration volumes across different infiltration formulations.

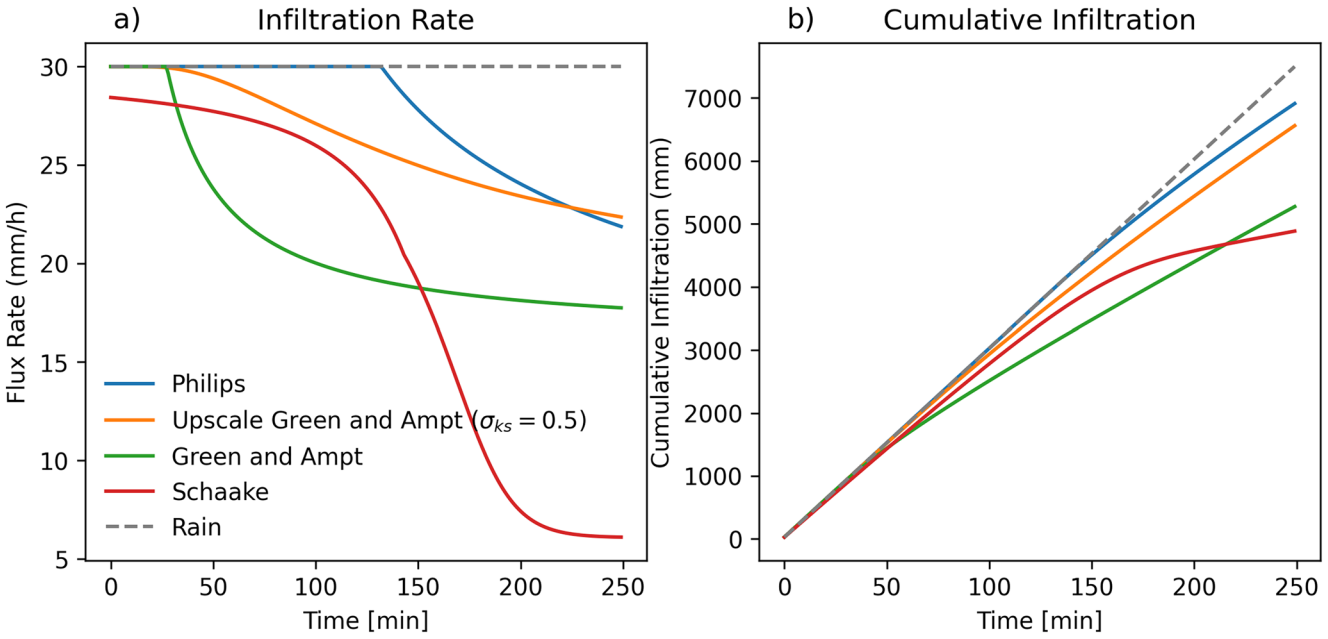


FIGURE A1 | (a) Temporal evolution of infiltration rates simulated by the infiltration approaches used in the main text: Philip (blue), Upscaled Green–Ampt (orange), Green–Ampt (green), and Schaake (red). (b) Cumulative infiltration over the simulation period. Rainfall intensity was held constant throughout the simulation at $i = 30\ \text{mm h}^{-1}$. The parameters used in the experiment were: Saturated hydraulic conductivity, $K_{sat} = 1.6\ \text{cm h}^{-1}$; saturated water content, $\theta_{sat} = 0.453\ \text{m}^3\ \text{m}^{-3}$; air-entry pressure at saturation, $\psi = 211.01\ \text{mm}$; pore-size distribution index, $\lambda = 4.9$ [−]; and standard deviation of saturated hydraulic conductivity, $\sigma_{K_{sat}} = 0.5$.

10991085, 2026, 10, Downloaded from https://onlinelibrary.wiley.com/doi/10.1002/hyp.70733 by NICE, National Institute for Health and Care Excellence, Wiley Online Library on [16/10/2026]. See the Terms and Conditions (https://onlinelibrary.wiley.com/terms-and-conditions) on Wiley Online Library for rules of use; OA articles are governed by the applicable Creative Commons License